Pharm Res (2012) 29:3213–3234
DOI 10.1007/s11095-012-0826-1

EXPERT REVIEW

Imaging of Cells and Nanoparticles: Implications for Drug Delivery to the Brain

Katica Stojanov • Inge S. Zuhorn • Rudi A. J. O. Dierckx • Erik F. J. de Vries

Received: 17 April 2012 / Accepted: 5 July 2012 / Published online: 18 July 2012

ABSTRACT A major challenge in the development of central nervous system drugs is to obtain therapeutic effective drug concentrations inside the brain. Many potentially effective drugs have never reached clinical application because of poor brain penetration. Currently, devices are being developed that may improve drug delivery into the brain. One approach involves the encapsulation of drugs into nanocarriers that are targeted to the brain, where the drug is released. Alternatively, living cells have been engineered to produce the pharmaceutical of interest at the target site. It is important to follow the fate of these drug delivery devices inside the body to verify their efficiency in reaching the brain. To this end, both *ex-vivo* approaches and *in-vivo* imaging techniques are used, including *ex-vivo* biodistribution, autoradiography, MRI, optical imaging, PET and SPECT. All these methods have their specific advantages and limitations. Consequently, selection of the tracking method should be based on the specific aims of the experiment. Here, we will discuss the methods that are currently applied for tracking brain drug delivery devices, including the most commonly used labels and labeling procedures for living cells and nanocarriers. Subsequently, we will discuss specific applications in tracking drug delivery devices.

KEY WORDS brain · drug delivery · imaging · nanocarriers · stem cells

K. Stojanov • I. S. Zuhorn
Department of Cell Biology / Membrane Cell Biology
University Medical Center Groningen, University of Groningen
A. Deusinglaan 1
9713 AV, Groningen, The Netherlands

R. A. J. O. Dierckx • E. F. J. de Vries (✉)
Department of Nuclear Medicine and Molecular Imaging
University Medical Center Groningen, University of Groningen
Hanzeplein 1
9713 GZ, Groningen, The Netherlands
e-mail: e.f.j.de.vries@umcg.nl

ABBREVIATIONS

[^{18}F]FDG	2′-[^{18}F]fluoro-2′-deoxyglucose
[^{18}F]FHBG	9-[4-[^{18}F]fluoro-3-(hydroxymethyl)butyl] guanine
[^{18}F]HFB	hexadecyl-4-[^{18}F]fluorobenzoate
[^{64}Cu]PTSM	[^{64}Cu]pyruvaldehyde-bis-(N4-methyl-thiosemicarbazone)
[^{99m}Tc]HMPAO	[^{99m}Tc]hexamethylpropyleneamine oxime
BBB	blood-brain barrier
BRET	bioluminescence resonance energy transfer
CED	convection enhanced delivery
CT	computed tomography
DOPE	1,2-Dioleoyl-sn-glycero-3-phosphoethanolamine
DTPA	diethylene triamine pentaacetic acid
eGFP	enhanced green fluorescent protein
FMT	fluorescence molecular tomography
GFP	green fluorescent protein
GRID	gadolinium rhodamine dextran
HSV-tk	thymidine kinase of herpes simplex virus
MRI	magnetic resonance imaging
NSCs	neural stem cells
PET	positron emission tomography
QDs	quantum dots
RFP	red fluorescent protein
SPECT	single photon emission tomography
SPIO	super-paramagnetic iron oxide
S-TRAIL	secreted form of an apoptosis inducing ligand
USPIO	ultra-small super-paramagnetic iron oxide
V_d	volume of distribution

INTRODUCTION

Many potential drugs for the treatment of brain diseases show excellent *in-vitro* effects, but do not reach application in patients. The high failure rate of initially promising drug

candidates is often caused by insufficient delivery of the drug into the brain, resulting in drug concentrations that are too low to be therapeutically effective (1). To enhance efficacy, a drug can be administered directly into the brain via intracerebroventricular or intracerebral injection. However, major drawbacks of these approaches are invasiveness and limited penetration of drug from the injection site toward surrounding brain tissue. Even when the delivery of the drug is facilitated by nanocarriers, the drug-penetrated tissue area is rather small. Consequently, intracranial injection of drugs is only suitable for treatment of brain disorders that are confined to a specific region within the brain, such as in primary brain tumors, stroke, and Parkinson's disease (2,3). Alternatively, brain delivery of drugs can be achieved via intravascular administration. This approach is much more patient-friendly and, once transported over the blood–brain barrier (BBB), the drug can literally reach every neuron in the brain (4). However, delivery of drugs from blood into brain is often hampered by poor penetration of the BBB, especially in case of hydrophilic and macromolecular drugs.

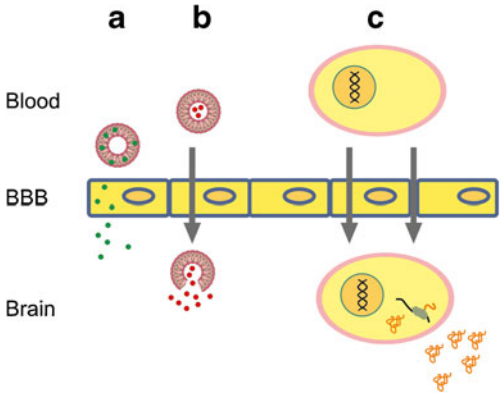

Fig. 1 Modes of facilitated drug delivery to the brain. (**a**) Lipophilic drugs are release from a nanocarrier in the blood compartment of the brain vasculature. The drug can subsequently penetrate the BBB by passive diffusion. (**b**) A nanocarrier loaded with the drug penetrates the BBB. Inside the brain parenchyma, the drug is released. (**c**) (Stem) cells are able to penetrate the blood brain barrier, especially at the site of injury. The cells can be genetically engineered with a gene that encodes for the therapeutic drug. Inside the brain parenchyma the cells will express the therapeutic gene and release the drug product.

DRUG DELIVERY (IN)TO THE BRAIN

Accumulation of a drug into the brain could theoretically be enhanced by administration of higher doses of the drug. This strategy, however, would also increase the exposure of peripheral organs, thereby enhancing the potential risk of toxic side effects. Therefore, different approaches to selectively increase drug accumulation in the brain have been developed (1). The first strategy relies on the incorporation or encapsulation of the drug into brain-targeting nanocarriers. When a lipophilic drug has to be delivered, binding of the drug-loaded nanocarrier to brain endothelium will suffice, as molecular exchange between nanocarrier and apical (blood-facing) cell surface will allow the drug to enter the brain via passive diffusion (Fig. 1). In case of hydrophilic or macromolecular drugs (e.g. proteins, peptides, oligonucleotides), the nanocarrier itself needs to cross the BBB and release its contents once it reaches the brain parenchyma. A second approach for improving drug delivery to the brain involves the use of living cells that are engineered to produce and secrete the pharmaceutical agent after cellular translocation across the BBB. This strategy primarily involves the use of (*ex-vivo*) genetically modified (neural) stem cells that have been shown to cross the BBB.

Nanocarrier-Mediated Drug Delivery

Nanocarriers are usually membrane-like vehicles with a diameter between 1 to 1000 nm that enclose an aqueous core. The membrane is often composed of a lipid bilayer (liposomes), or amphiphilic synthetic block copolymers (polymersomes). Alternatively, nanocarriers without an aqueous core have been prepared, such as solid lipid nanoparticles and solid polymeric nanoparticles. Besides these artificial drug delivery devices, exosomes, i.e. vesicular structures of 40–80 nm produced by distinct cell types, were recently also reported as delivery vehicles for siRNA (5). The potential of using nanocarriers as drug delivery devices for the brain has been extensively reviewed by Tiwari and Amiji (6). Intrinsically, nanocarriers do not selectively target to the brain. Therefore, specific peptides or antibodies that selectively recognize endothelial cell surface receptors, capable of engaging into transcytotic transport mechanisms, can be coupled to the nanocarriers. In this manner, transport of the carrier across the BBB would be specifically facilitated, leading to an enhanced delivery of the drug into the brain. Of potential interest in this regard are transferrin, insulin and the dodecapeptide G23, which are transported across the BBB via receptor-mediated transcytosis (7–9). Hence, nanocarriers specifically engineered in this manner, and displaying BBB transcytotic capacity following systemic administration, may hold great promise for the treatment of multifocal brain diseases, including brain metastases, multiple sclerosis, Alzheimer's disease, and amyotrophic lateral sclerosis (10).

Cell-Based Drug Delivery

Many studies in animal models have shown that neural stem cells migrate to sites of brain injury caused by e.g. a tumor (11), neurodegeneration (12) or cerebral ischemia (13). In these cases, stem cells transduced with a therapeutic gene

could be an alternative strategy for drug delivery to the pathologic brain (14). These engineered stem cells are either injected into a peripheral vein or directly transplanted into the brain by intracerebral or intraventricular injection. After administration via intravenous injection, the number of cells reaching the brain may be relatively small (11), because the cells are trapped in the capillary network of internal organs, in particular in the lungs (15–17). In addition to capillary trapping, an interaction of the administered cells with cells of the reticuloendothelial system likely also plays a role in cell trapping, particularly in liver and spleen (15). However, it has also been shown that the capillary trapping can be alleviated using vasodilators (17,18). Thus this stem cell-based approach warrants further exploration of the possibilities to optimize the number of stem cells that reach the brain upon intravascular administration, especially since prolonged secretion of a drug from (genetically engineered) stem cells in the brain may result in therapeutic levels of the drug.

MONITORING TRAFFICKING OF DRUG DELIVERY DEVICES

To monitor the efficacy of delivery devices for brain-destined drugs, physiological effects induced by the drug in the brain could be monitored as surrogate endpoints of drug concentration (19,20). Such indirect measurements of drug delivery efficiency, however, would be prone to many confounding factors and therefore are usually not very sensitive. A more direct approach would be to measure the concentration of the nanocarrier itself, as a measure of transcytotic efficiency, or the concentration of the drug, as a measure of delivery/release inside the brain. Obviously, an adequate and sensitive methodology to track nanocarriers is required to determine brain delivery efficiency of these devices. Several *in vivo* and *ex vivo* approaches have been applied so far.

Ex vivo detection of drug delivery devices in brain involves the isolation of the brain, followed by biodistribution studies, autoradiography or fluorescence microscopy (21–23). In general, *ex vivo* detection is commonly applied in animal studies, although human post mortem material can occasionally also be used (24). With appropriate (immuno)histological labeling of brain tissue, the exact position of drug delivery devices relative to the different brain structures and cell types can be determined (25). A major disadvantage of *ex vivo* detection methods is that the kinetics of drug delivery device trafficking cannot be monitored in a longitudinal fashion.

In vivo detection methods are noninvasive and therefore allow multiple imaging sessions that may provide information on the changes in the distribution of nanocarriers and their contents within a living organism over time. *In vivo* imaging of nanocarrier trafficking requires modification of the device with a label that can be detected outside the body. Drug delivery devices can be tracked *in vivo* over several hours, when labeled with short-lived radioactive isotopes (17), or up to several weeks or months, when labeled with magnetic beads or reporter genes (26). Labeling of both the drug delivery device and the loaded drug enables simultaneous assessment of the fate of the carrier and the drug, thus providing information on delivery device integrity and concomitant drug release (27). Moreover, *in vivo* imaging can help to determine the optimal application route and dosing regimens of the therapeutics.

In the next sections, we will briefly discuss the most relevant noninvasive imaging methods currently applied for monitoring migration of drug delivery devices.

NONINVASIVE IMAGING METHODS

Magnetic Resonance Imaging (MRI)

MRI is a high-resolution imaging technique that provides excellent soft tissue contrast (28). In MRI, nuclei in a magnetic field are excited to a high energy spin state by a radiofrequency pulse. When these nuclei return to their low energy spin state, the electromagnetic flux is measured and converted into images. Two types of MRI images can be acquired: T1 and T2-weighted MRI. T1-weighted MRI is based on the longitudinal (realignment) relaxation time of the excited nuclei, whereas T2-weighted MRI is based on the transverse (spin phase) relaxation time. The signal of both T1 and T2-weighted MRI depends on the interaction of the relaxating nucleus with its immediate environment. MRI usually measures the spin relaxation of protons present in water. However, other atoms like ^{13}C, ^{23}Na and ^{31}P can also be used for MRI, but these atoms generate a much weaker signal and are far less abundant *in vivo* than ^{1}H. For *in vivo* tracking of specific probes, different contrast agents have been applied to label cells and molecules of interest (29). Two classes of contrast agents can be distinguished: paramagnetic and super-paramagnetic. Paramagnetic contrast agents, usually gadolinium complexes, enhance the signal in T1-weighted MRI, whereas super-paramagnetic contrast agents like iron oxide particles reduce the T2 signal (Fig. 2). Super-paramagnetic contrast agents generally generate a stronger signal than gadolinium and are therefore often more sensitive.

Optical Imaging

Fluorescence and bioluminescence imaging are widely applied optical imaging techniques today (30,31). In fluorescence imaging, an external light source excites a fluorescent probe inside an animal to a higher energy state. The fluorescent probe subsequently returns to its

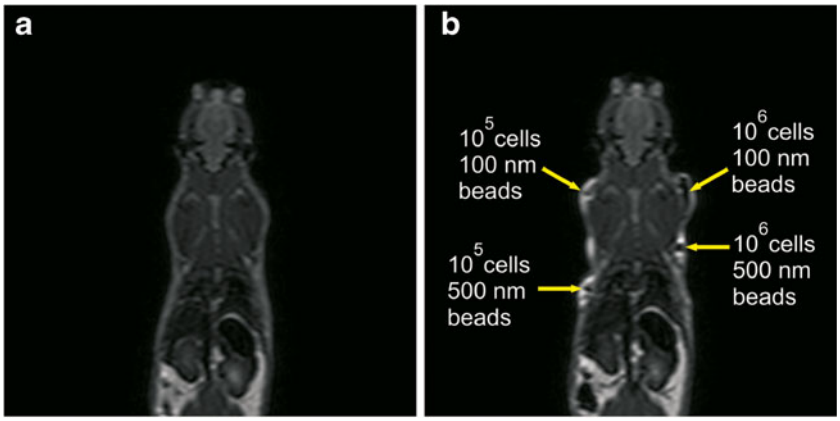

Fig. 2 T2-weighted MRI of C17.2 neural stem cells labeled with iron oxide beads, subcutaneously injected in rats. (**a**). Control rat. (**b**). Rat subcutaneously injected with 10^5 and 10^6 C17.2 neural stem cells that were labeled with 100 nm fluidMAG-UC and 500 nm screenMAG-hydroxyl beads. (images were kindly provided by K. Stojanov and I.S. Zuhorn).

ground energy state by emission of light with a longer wavelength (31). The emitted light is detected outside the animal by a light sensitive camera. When multiple fluorescent probes are used that emit light at different wavelengths, various processes can be studied simultaneously using appropriate light filters. The major limitations of fluorescence imaging are the contribution of autofluorescence by tissue and poor penetration of light through tissue (32). Therefore, fluorescence imaging is mainly suitable for application in small animals. Two-dimensional optical images preferentially show superficial activity and cannot resolve depth. The nonlinear attenuation of light by tissue makes quantification of optical imaging data a complicated task. Tomographic optical imaging devices have now been developed to overcome these limitations (33). Improved quantification and volumetric localization can be achieved using transmission images that can be generated with light source-detector pairs at multiple angles (34).

In bioluminescence imaging (35), animals or specific cells have been engineered to express a light-producing enzyme (luciferase). Firefly luciferase is the most frequently used enzyme for bioluminescence imaging. In the presence of oxygen and adenosine triphosphate, firefly luciferase oxidizes its substrate luciferin, and produces yellow-green light with an emission peak of approximately 560 nm. Luciferases of other species, such as click beetle, and luciferases that react with different substrates, such as sea pansy (Renilla) and marine copepod (Gaussia), have also been used (36). Bioluminescence of firefly luciferase generates an emission spectrum of which about 30% is above 600 nm. Although a major portion of the light signal is absorbed and scattered by tissue, the low background associated with bioluminescence makes this technique more sensitive than fluorescence imaging.

Nuclear Imaging

Positron emission tomography (PET) and single photon emission computed tomography (SPECT) are nuclear imaging techniques that can provide functional information about biochemical and physiological processes. Both PET and SPECT imaging are based on the detection of radiation emitted by an intravenously injected radioactive tracer using a dedicated camera (37,38). PET and SPECT differ in the radionuclide that is employed to label the tracer and in the detection technology of the camera.

PET isotopes, such as ^{11}C, ^{18}F and ^{89}Zr, decay by emission of a positron, which travels a short distance in tissue. When the positron has lost most of its energy, it annihilates together with an electron, resulting in the formation of two 511 keV photons. These photons are emitted at an angle of 180° and are detected outside the body by the PET camera. PET is highly sensitive, as detection sensitivity is in the picomolar concentration range. In PET, absorption of radiation by the body can be compensated for by attenuation correction, using a transmission scan that is made with an external radioactive source or a CT scan (for hybrid systems). A major advantage of PET over other imaging techniques is that it allows absolute quantification of the biochemical parameter of interest by pharmacokinetic modeling.

SPECT imaging uses probes that are labeled with radionuclides that emit single photons, such as ^{99m}Tc, ^{111}In and ^{123}I. For localization of the origin of the photons, a collimator is placed between the subject and the detector system. A collimator is a perforated plate - usually lead or tungsten - that can only be penetrated by photons that travel in the same direction as the channels in the collimator. Because the collimator blocks most photons, the sensitivity of SPECT is about 2 orders of magnitude lower than that of PET. In most systems, the collimator and detector rotate around the subject in order to obtain data in three dimensions. Quantification of SPECT data is a major technological challenge (39). Nevertheless, in contrast to PET, multiple energy windows can be used in SPECT, which allows simultaneous imaging of different probes labeled with different isotopes.

LABELING METHODS

Since drug delivery devices generally do not display intrinsic properties that allow their *ex vivo* detection or *in vivo* imaging,

it is usually necessary to tag the drug carriers with a suitable label to enable tracking of their *in vivo* distribution. Depending on the detection or imaging tool used, several labeling methods are available. Before discussing specific applications, we will first briefly highlight the most commonly used procedures to label delivery vehicles– being either cell-based or artificial nanocarriers – as applied in brain delivery.

Direct Labeling Methods for Cell-Based Drug Delivery Devices

Cell Labeling with MRI Contrast Agents: Gadolinium Complexes

For the purpose of cell tracking in the brain, neural stem cells have been labeled with various gadolinium-based contrast agents, such as gadolinium-diethylene triamine pentaacetic acid (Gd-DTPA) and gadopentetate dimeglumine (40,41). After labeling, more than 90% of the stem cells were still viable, as determined by a Trypan blue exclusion assay. The Gd-DTPA label could still be detected in the stem cells *in vitro* for up to 2 weeks after labeling. Modo *et al.* labeled immortalized stem cells with a bimodal fluorescent MRI contrast agent, called gadolinium rhodamine dextran (GRID), consisting of rhodamine and gadolinium-DTPA chelates that are covalently attached to a 10 kDa dextran molecule (42). Cell viability in the presence of GRID was largely unaffected. However, cell division resulted in a dilution of the GRID signal and as a consequence, the rhodamine signal could not detected anymore at day 7 after labeling, while the gadolinium signal allowed for detection of cell migration by MRI for up to 14 days after grafting in a rat middle cerebral artery occlusion model (43). These results likely reflect the differences in intrinsic sensitivities of the detection techniques. Giesel *et al.* showed that primary human mesenchymal stem cells can be readily labeled with Gadofluorine M, a macrocyclic gadolinium-based contrast agent with a perfluorinated side-chain. *In vitro*, the label was detectable inside the cells for an impressive period of 6 weeks (26). However, in this study important data on cell proliferation and cell viability are lacking.

Cell Labeling with MRI Contrast Agents: Iron Oxide Particles

Super-paramagnetic iron oxide (SPIO) particles consist of a crystalline iron oxide core and a shell of hydrophilic polymer. Under normal conditions, these iron oxide particles can be taken up by cells via endocytosis. However, undifferentiated (stem) or less differentiated (progenitor) cells do not have the full endocytic capacity that is necessary for an efficient intracellular accumulation of iron oxide particles. To overcome this problem, the internalization of iron oxide particles by these cells has been improved by employing technologies developed for DNA transfection, such as the use of the commercially available delivery agents Lipofectamine, poly-L-lysine, protamine sulfate, Metafectene, JetPEI and Fugene (44, 45, Stojanov unpublished). The ratio of SPIO to delivery agent and the total amount of iron in the medium is critical for the efficiency of internalization of iron into the cells (44). In general, cell labeling protocols for iron oxide particles have to be optimized in a cell dependent manner for each combination of iron oxide particle and delivery agent (45) in order to optimize a balance between delivery efficiency and toxicity (46). The ultra small SPIO (USPIO) Sinerem, for example, was stably incorporated in D3 embryonic stem cells and C17.2 neural stem cells in the presence of Metafectene, but D3 embryonic stem cells were less tolerant to high concentration of the transfection agent (47). Cells stably labeled with SPIOs in the presence of a delivery agent could be detected by MRI *in vitro* for up to seven doubling cycles (47) and *in vivo* for at least 3 weeks (48,49).

Electroporation represents an alternative method to improve iron particle internalization by cells. When appropriate electroporation settings are used, sufficient amounts of Feridex (Endorem) can be incorporated into C17.2 neural stem cells for *in vivo* imaging (50). Using optimized conditions, cell viability and differentiation capacity *in vitro*, and proliferation and migration of the cells *in vivo* were maintained. As Feridex is an FDA-approved agent this method can be readily translated into a clinical setting.

Iron oxide particles in the micrometer size range were also suggested as possible contrast agents. The high amount of iron present in one particle already gives a detectable signal, which makes single particle imaging possible (51). The size of the particle, however, can strongly influence the stability of the label in a proliferating cell population. Whereas 0.9 μm iron oxide particles were evenly distributed between daughter cells of labeled mesenchymal cells (52), 1.6 μm particles showed a tendency to be secreted by cells after long-term culturing and were unevenly distributed between daughter cells, leaving some of the cells without contrast agent (47). The use of these larger iron particles for cell labeling therefore needs to be validated for each cell type.

Cell Labeling with Fluorescent Probes: Quantum Dots

Semiconductor nanocrystals (quantum dots) are a new class of fluorescent probes with high quantum yield and resistance to photobleaching. Quantum dots (QDs) are characterized by size dependent absorption and emission (53). Cells can be labeled with QDs via spontaneous internalization. Similar to iron oxide particles, QDs labeling efficiency can be improved by electroporation and conjunction with compounds employed in DNA delivery like cationic lipids or polymers. In addition, the use of a specific targeting peptide has been described to improve QD cell labeling efficiencies (53). When ES-D3 murine embryonic stem cells were labeled with peptide

based QD QTracker, 72% of the cells contained QDs after 24 h , but only 4% of the cells remained positive at day 4 (54). The authors argued that the loss of signal could be a consequence of fast cell division and/or active secretion of QDs from the cells. In contrast, the QD signal could be visualized *in vivo* for up to 14 days after subcutaneous administration of the labeled cells. However, histological analysis revealed that QDs were present in surrounding host cells rather than the teratomas that had grown from the embryonic stem cells. This finding suggests that QDs were secreted from embryonic stem cells and subsequently taken up by neighboring host cells. This study underlines the importance of determining whether the probe is stably incorporated inside the labeled cell, especially in long term cell tracking experiments *in vivo*.

Similar to any other fluorescent probe, excitation of QDs is hampered by light absorption and scattering by tissues, leading to inefficient excitation of the fluorescent label particularly when present in deep tissue. In order to overcome this drawback, QDs that do not require external light for activation have been designed (55) based on a process called bioluminescence resonance transfer energy (BRET). In this approach, Luc8 luciferase was coupled to QD655 (QD with an emission wavelength of 655 nm). When the substrate coelenterazine is added, Luc8 luciferase emits light with a maximum intensity at 480 nm, which excites QD655. The QD will subsequently emit light at 655 nm, which has better tissue penetration than the light emitted by luciferase. BRET emission (at 655 nm) is more readily detected than luciferase emission, particularly in deep tissues. Indeed, C6 glioma cells that are labeled with QD655-Luc8 could be visualized in lungs by application of the BRET technology, but not by fluorescence. However, a potential obstacle for application of BRET for brain imaging is that luciferase substrates do not readily cross the BBB (56).

Cell Labeling with Radioactive Probes: PET Tracers

The glucose analogue 2′-[^{18}F]fluoro-2′-deoxyglucose ([^{18}F]FDG) is a widely available and extensively used PET tracer. [^{18}F]FDG enters the cell via GLUT transporters and is subsequently phosphorylated by hexokinase. [^{18}F]FDG 6-phosphate no longer permeates across the cell membrane and remains therefore trapped inside the cell. With a half-life of 110 min, [^{18}F]FDG can be used only for short-term cell tracking (4–6 h). [^{18}F]FDG does not induce long-term radiotoxicity (57). However, efflux of [^{18}F]FDG from stem cells (17,57), T lymphocytes (58) and C6 rat glioma cells (59) is significant over time. This efflux is probably due to dephosphorylation of [^{18}F]FDG 6-phosphate by glucose phosphorylase, followed by release of free [^{18}F]FDG. *In vivo* released [^{18}F]FDG can be taken up by various tissues with a high glucose metabolism, which result in a high background signal (Fig. 3). *In vitro,* the efflux of [^{18}F]FDG can be partly inhibited by the glucose transporter inhibitor phloretin (17). *In vivo*, however, a bolus administration of this GLUT inhibitor could not completely prevent loss of radioactive tracer from the labeled cells. Since phloretin is also a vasodilator, it did prevent the trapping of the labeled cells in the lung capillaries.

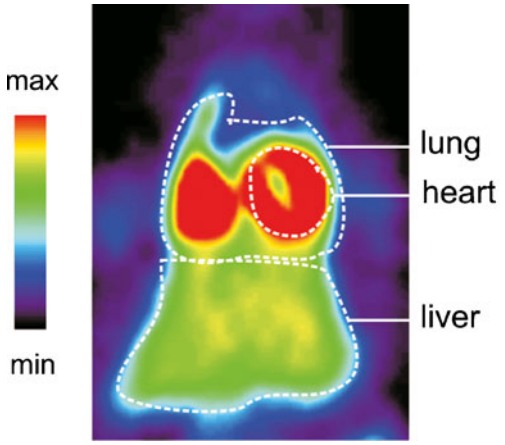

Fig. 3 A PET image (coronal section) showing distribution of [^{18}F]FDG labeled C17.2 cells in lung and liver 1 h after i.v. administration in rat. [^{18}F]FDG released by C17.2 cells is taken up by the heart.

An alternative labeling method for short term cell tracking with PET is labeling of the cells with hexadecyl-4-[^{18}F]fluorobenzoate ([^{18}F]HFB). [^{18}F]HFB was used for labeling of mesenchymal stem cells by intercalation of the tracer in the cell membrane (60). More than 90% of the incorporated [^{18}F]HFB was retained in the cells 4 h after labeling, compared to only 60% for [^{18}F]FDG (57). Accordingly, [^{18}F]HFB seems to be a more appropriate tool for short term tracking of cells with PET than [^{18}F]FDG.

For cell tracking over a period of 24-36 h, the PET tracer [^{64}Cu]pyruvaldehyde-bis-(N4-methyl-thiosemicarbazone) ([^{64}Cu]PTSM; half-life 12.7 h) was suggested (59), but a variety of cell types labeled with this tracer showed significant efflux of radioactivity over time (59,61,62). As an alternative, stem cells could be labeled with [^{64}Cu]tropolone in the presence of the membrane-permeable divalent chelator 2-(2-amino-4-methyl-5-flurophenoxy)methyl-8-amino-quinoline-N,N,N',N'-tetra-acetic acid. This method gives high labeling efficiency for human leukocytes and 80% retention 24 h after labeling (63). However, attempts to label stem cells using this technique have not been reported yet.

Cell Labeling with Radioactive Probes: SPECT Tracers

[^{99m}Tc]hexamethylpropyleneamine oxime ([^{99m}Tc]HMPAO; [^{99m}Tc]exametazime; half-life 6 h) is the radiopharmaceutical of choice for leukocyte labeling. It allows tracking of labeled cells up to 24 hours. Only few attempts to radiolabel stem cells with [^{99m}Tc]HMPAO have been

described thus far. We labeled murine C17.2 neural stem cells with [^{99m}Tc]HMPAO at a concentration of 5 MBq/10^6 cells without any sign of acute toxicity. However, leakage of radioactivity from the stem cells was about 20% after 2 h (unpublished data). Also mesenchymal stem cells have been labeled with [^{99m}Tc]HMPAO (64). Although no labeling details were provided, release of ^{99m}Tc from these cells apparently also occurred, as can be inferred from the high radioactivity that was measured in the kidney and bladder. Therefore, proper control experiments should be conducted to discriminate whether the observed radioactivity in an organ originates from intact labeled cells, or from released ^{99m}Tc.

Next to [^{99m}Tc]HMPAO, [^{111}In]oxine has frequently been used for leukocyte radiolabeling. With a half life of 2.8 days, [^{111}In]oxine labeling should in theory allow the monitoring of cell distribution for over a week. [^{111}In]oxine was also used for labeling of several types of progenitor cells, but with various degrees of success. Murine hematopoietic progenitor cells proved to be sensitive to labeling with [^{111}In]oxine, as significant toxicity was observed when either 1 MBq or 0.1 MBq of tracer was applied per million cells (65). The maximum dose of [^{111}In]oxine that did not affect canine bone marrow-derived mesenchymal stem cell survival and function was 0.14 MBq/10^6 cells (66). In contrast, human mesenchymal stem cells could be labeled with 7.5 MBq/10^6 cells without affecting the doubling time and differentiation into endothelial cells (67). Human endothelial cells could even be labeled with [^{111}In]oxine at a concentration of 10 MBq/10^6 cells without changing viability or migration capacity (68). In contrast, labeling of human hematopoietic progenitor cells with a similar dose of [^{111}In]oxine abolished cell viability and differentiation 7 days later (69). Thus, there appears to be a strong variability in sensitivity towards [^{111}In]oxine between cell types, with a tendency of a higher sensitivity for less differentiated cells. The mechanisms of cell damage have not been revealed yet, but probably include heavy metal poisoning, high radiosensitivity of cell lines, and cell handling during the labeling procedure (69,70). Loss of radiolabel is another problem for cell labeling. Cellular retention of [^{111}In]indium 48 h after labeling of dendritic cells, and hematopoietic and endothelial progenitor cells ranges from 18 to 39% (65,68,71) depending on cell type and experimental settings. Despite the efflux of many radiotracers, direct radiolabeling of cells still allows for short term cell tracking and a comparative analysis of the availability of cells at the target site, for example, following different routes of administration.

The effects of the different labeling methods on cell viability are summarized in Table I.

Reporter Gene-Mediated Labeling Methods for Cell-Based Drug Delivery Devices

Besides direct labeling of the cells, monitoring of cell trafficking can also be accomplished by introducing a so-called reporter gene within the cell of interest. Thus a reporter gene can be co-expressed together with a therapeutic gene in order to monitor cell migration and while applying gene therapy. Products of reporter genes can be directly detected (e.g. a produced fluorescent protein) or by functional assays in case the reporter gene leads to the expression of receptors, transporters or enzymes, which involves indirect means of detection. In the latter case an external probe has to be introduced in order to 'sense' reporter gene expression. When stably incorporated into the cell genome, reporter genes can in principle be continuously expressed and therefore they can be detected perpetually. In sharp contrast, transient transfection will result in loss of signal over time, because of dilution of the gene product during subsequent rounds of cell division. However, it has been noticed that, even in case of stable transfection, expression of reporter genes in stem cells can be silenced over time, which is usually caused by promoter methylation (72).

Reporter Genes for MRI

A novel and emerging class of reporter genes are those that rely on detection by MRI (73). Recently, it was shown that overexpression of the iron storage protein ferritin in cells leads to an increased but non-toxic iron accumulation that is sufficient for noninvasive imaging (74,75). Zurkiya *et al.* investigated the magnetotactic bacterial gene, MagA, that is coding for the H^+/Fe(II) antiporter (76,77) and responsible for the formation of SPIO-like nanoparticles within cells (78). MagA expression in the human embryonic kidney cell line 293FT resulted in the intracellular formation of non-toxic magnetic nanoparticles and MagA-transfected cells could be detected by MRI *in vivo* following their implantation in the brain (78).

Reporter Genes for Fluorescence Imaging

Fluorescent proteins are probably the most frequently used reporters. For *in vitro* use, variants of fluorescent proteins with emission wavelengths in the visible spectrum (400-600 nm), such as GFP and red fluorescent protein (RFP), were developed (Table II). Due to strong tissue (hemoglobin) absorption of light with wavelengths below 600 nm, most of the fluorescent proteins that have been designed for *in vitro* use cannot be used for cell tracking *in vivo*, because only superficial targets (<1 cm deep) can be imaged with these probes. Therefore, fluorescent probes that emit light with wavelengths between 600 nm and 900 nm, i.e. in the near-

Table I Effect of Labeling Reagents or Methods on Cellular Toxicity

Imaging technique	Label	Effect on labeled cells	Remarks	References
MRI	Gadolinium compounds • Gd-DTPA • Gadopentetate • Dimeglumine • Gadolinium rhodamine dextran	Cell viability largely unaffected		(40–42)
	• Gadofluorine M	Data are lacking		(43)
	Iron oxides • USPIO • SPIO • MPIO	Non-toxic	Excess of transfection agent can be toxic	(44,46,47,50–52)
Fluorescence imaging	• Fluorescent proteins	(Over)expression might be toxic	Effect on stem cells is unknown	(156–158)
	• Quantum dots	Cell toxicity largely unknown		
Bioluminescence imaging	• Luciferases	Non-toxic for tumor cells	Effect on stem cells is unknown	(159)
SPECT	• ^{99m}Tc-HMPAO	No acute toxicity		(64,160)
	• ^{111}In-oxine	Ranges from no effect on doubling time to abolishing cell viability and differentiation depending on dose, cell type and degree of differentiation	Toxicity is a combination of heavy metal poisoning, cell radiosensitivity and handling during labeling procedure	(65–69)
PET	• ^{18}FDG	No long term radiotoxicity		(57)

infrared range, are preferred for *in vivo* imaging (79). Above 900 nm, light absorption by water molecules begins to interfere. Therefore, over the past 10 years several red and near-infrared emitting proteins, suitable for *in vivo* application, have been developed (Table II). Besides the development of better probes, scientists have also developed three dimensional reconstruction methods tailored for *in vivo* imaging of near-infrared proteins. In this manner, the imaging sensitivity of tumor cells was increased by an order of magnitude when mCherry is used as reporter gene, as compared to eGFP (80). This approach also improved the accuracy of localization and measurement of the size of a mCherry-expressing tumor implanted in the brain. These results warrant future studies to examine the potential of near-infrared fluorescent proteins for *in vivo* tracking of stem cell migration into the brain and for long term expression of potential therapeutics produced by these stem cells.

Reporter Genes for Bioluminescence Imaging

In bioluminescence imaging, luciferases with bioluminescence above 600 nm are preferred, because tissue absorption and scatter are lower at these wavelengths. Up to now, firefly luciferase (Table III) is the most frequently used

Table II Optical Characteristics of Fluorescent Proteins Suitable for *In Vivo* Application Compared to GFP. Modified from Deliolanis *et al.* 2008 (161)

Protein (Acronym)	Excitation Maximum (nm)	Emission Maximum (nm)	Molar Extinction Coefficient	Quantum Yield	Relative Brightness (% of EGFP)	ref
EGFP	489	509	53	0.60	100	(162)
tdTomato (Tandem)	554	581	138	0.69	283	(163)
mCherry	587	610	72	0.22	47	(163)
mRaspberry	598	625	86	0.15	38	(164)
mRFP	584	607	50	0.25	37	(163)
mPlum	590	649	41	0.10	12	(164)
Katushka	588	635	65	0.34	62	(165)

Table III Properties of Bioluminescent Reporter Proteins

Luciferase	Species	Substrate	Peak emission wavelength (nm)	NB	ref
Firefly	*Photinus pyralis*	D-luciferin	562 (550-620*)	* Mutants with various emission maximums exist	(81,166*)
Click beetle	*Pyrophorus plagiophthalamus*	D-luciferin	546, 560, 578, 593		(167)
Renilla	*Renilla reniformas*	Coelenterazine	480, 547		(168,169)
Gaussia	*Gaussia princeps*	Coelenterazine	480	Naturally secreted. Probably restricted passage across the BBB (170)	(171)
Bacterial luciferase	*Photorhabdus luminescens*	Endogenously produced	490	Codon-optimized for expression in human cell lines	(86)

luciferase, because it emits light in this range. An overview of the various applications, advantages and disadvantages of the use of luciferases *in vivo* are reviewed elsewhere (81,82). An example of the use of luciferase as a reporter gene for bioluminescence imaging of neuronal stem cells is given in Fig. 4. Longitudinal bioluminescence imaging was applied to monitor the survival of luciferase and GFP expressing neural stem cells after stereotactic injection in corpus callosum (83). Because of the limited resolution of bioluminescence, fluorescence microscopy of the co-expressed GFP reporter gene was subsequently applied to detect the location of the stem cells.

Due to tissue attenuation and light scattering, bioluminescence imaging does not allow absolute quantification of the signal. Moreover, bioluminescence imaging in the brain is hampered by the fact that the luciferase substrates luciferin (for firefly and click beetle luciferase) and coelenterazine (for Renilla and Gaussia luciferase) are efficiently removed from the brain by the ABC transporters ABCG2 and ABCB1 at the BBB (56,84). In contrast to eukaryotic luciferases that are encoded by one gene, bacterial luciferases are encoded by a cassette of 5 genes, the Lux operon. A luciferase dimer is encoded by genes luxA and luxB, whereas the other three genes (luxC, D and E) encode for the required enzyme substrate (85). Since both luciferase and its substrate are the product from the same operon, external application of the substrate is not required. This feature makes the Lux operon highly attractive for cell tracking in the brain. Recently stable expression of the codon-optimized Lux operon in the human HEK293 cell line has been reported (86). However, the potential of this expression system in brain research remains to be explored.

Reporter Genes for Nuclear Imaging

Many PET and SPECT reporter probes (Table IV) have been developed over the past years (87). However most of

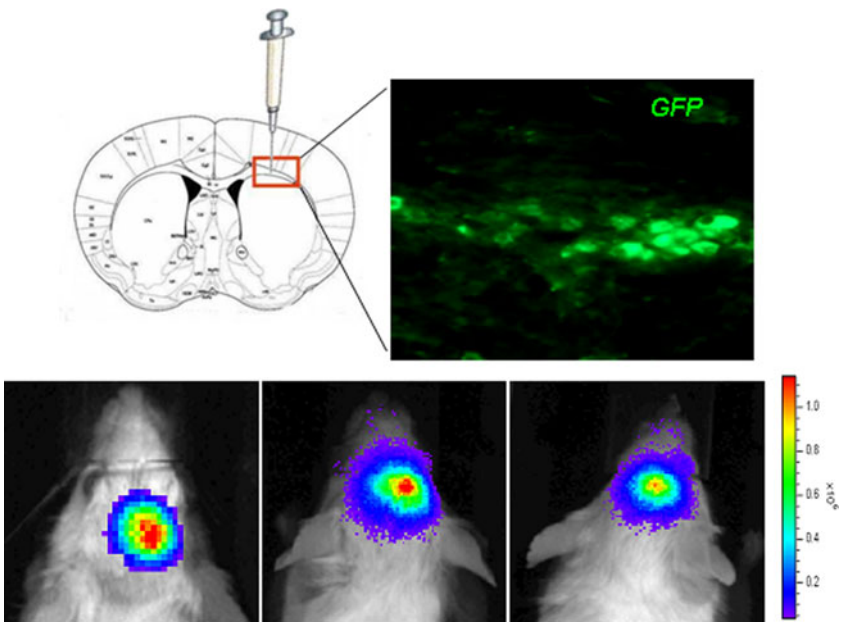

Fig. 4 Luciferase-GFP-actin transgenic neural stem cells, primed to become oligodendrocytes, were stereotactically injected in the demyelinated corpus callosum of a cuprizone-fed mouse. Bioluminescence imaging at 3, 5 and 8 weeks after implantation, reveals their survival. The specific location of the implanted cells was validated by GFP – histochemistry (images were kindly provided by Dr. J.C.V.M. Copray).

Table IV Available Reporter Genes for PET and SPECT Imaging

Reporter gene	Reporter probe	Radioisotope	Reporter probe crosses intact BBB	NB	ref
Herpes simplex virus type-1 thymidine kinase (HSV1-tk)	Various pyrimidine and acycloguanosine derivatives	^{11}C, ^{18}F, ^{124}I, ^{131}I – PET ^{123}I, ^{125}I - SPECT	no		(172)
Dopamine D_2 receptor (D_2R)	Fluoroethylspiperone (FESP)	^{18}F - PET	yes	Large background signal in the striatum	(173)
Dopamine transporter (DAT)	TRODAT-1	^{99m}Tc -SPECT	yes	Large background signal in the striatum	(174)
Sodium-iodide symporter (NIS)		^{99m}Tc-pertechnetate, ^{125}I - SPECT	no		(175)
Somatostatin receptor	Octreotide P2045 P829	^{111}In, ^{99m}Tc - SPECT	no		(176,177)
E.coli xanthine phosphoribosyltransferase (XPRT)	Xanthine		yes	Unavailable radiolabeled reported probe	(178)
Human cannabinoid receptor 2 deficient for signal transduction hCB_2(D80N)	GW405833	^{11}C – PET	yes	Background signal from activated microglia?	(88)

them fail to cross the intact BBB. On the other hand, probes that can cross the BBB, such as probes for the D2 receptor, may not be suitable for reporter gene imaging, because of a high basal expression level of the endogenous receptor in the brain.

Recently, hCB_2(D80N), a human gene encoding the cannabinoid receptor-2 which is deficient for signal transduction, has been introduced for imaging gene expression behind the intact BBB (88). CB_2 has low endogenous brain expression. Brain adenoviral overexpression of hCB_2(D80N) was visualized using [^{11}C]GW405833, a CB2-selective partial agonist that crosses the BBB. Nevertheless, the potential to use this system for stem cell tracking in the brain (89) requires further investigations. In fact, a potentially perturbing factor in applying this reporter gene system is that expression of CB_2 is upregulated by activated microglia during inflammation. Since many brain disorders are accompanied by activation of microglia, it might therefore be difficult to discriminate between cell migration *versus* microglia activation, using this reporter gene at disease conditions.

Labeling Methods for Nanocarriers as Drug Delivery Devices

Liposomes are classical nanoparticulate drug delivery devices. Not surprisingly therefore, most of the labeling techniques have been developed for liposomes. Some of these techniques have later been adopted for labeling of other nanoparticles (Table V). In principle, there are three approaches for liposome labeling. In the first approach, hydrophilic tracers are trapped in the aqueous core of the liposome, while lipophilic tracers become trapped within the lipid bilayer. In the second strategy, the tracer is covalently coupled to the liposomal membrane. The third approach involves non-covalent binding of the tracer to a chelator that is covalently coupled to the membrane. The stability of labeled nanoparticles is usually examined *in vitro* by incubation in buffer and plasma for an extended period of time, followed by determination of the presence of free label and/or nanoparticle metabolites, using ITLC or column chromatography. However, due to dilution effects and shear stress in blood, variations in microenvironment, clearance (i.e. interaction with cells of the reticuloendothelial system, renal and biliary clearance), *in vivo* stability of labeled nanoparticles may substantially differ from their stability observed *in vitro*.

Nanocarrier Labeling with MRI Contrast Agents

Of all potential brain drug delivery devices, only liposomes have been labeled with gadolinium chelates to obtain MRI contrast. Gadolinium contrast agents can be incorporated into liposomes by several cycles of freeze-thawing followed by extrusion through filters in order to obtain liposomes of a homogeneous and well-defined size. In this way, gadolinium-DTPA, gadodiamide and gadoteridol have been incorporated in liposomes (90–92). Alternatively, a gadolinium chelator such as DTPA has been covalently

Table V Overview of the Labeling Methods Reported for Nanocarriers

Imaging modality	Label	Labeling technique	Type of nanocarrier	Remarks	References
MRI	• Gd-DTPA • Gadodiamide	Trapping in the aqueous core	Liposome		(90–92)
	• Gadoteridol				
	• Gd-DTPA-lipid	Chelation	Liposome	Large density of DTPA on liposome surface required	(93)
	• Magnetic nanoparticles	Reverse phase evaporation	Liposome		(95,96)
	• Magnetic nanoparticles	Film hydration	Polymersome		(97,98)
Fluorescence imaging	• DiI • N-Rh-PE	Lipid analogs	Liposome		(99)
	• Dy-676-C_{18} • Cy7.5-DOPE	Covalent coupling	Liposome	Also applicable on polymersomes	(102,103)
	• 6-coumarin	Trapping in shell	Liposome / Polymersome		(32,100,101)
SPECT	• ^{111}In-DTPA	Trapping in aqueous core by trans-chelation	Liposome		(105)
	• ^{111}In-DTPA-PE	Chelation	Liposome	Also applicable on polymersomes	(106)
	• ^{99m}Tc-etoposide • ^{99m}Tc-Docetaxel	Trapping in by trans-chelation	Polymersome / Solid lipid nanoparticle	Also applicable on liposomes	(109,110)
PET	• ^{64}Cu-BAT-PEG-lipid	Chelation	Solid lipid nanoparticle		(108)

coupled to a lipid that is incorporated into the liposome bilayer (93). Subsequent addition of gadolinium will then assure its binding to the liposomal surface via chelation by the DTPA-derivatized lipid analogue. Interestingly, localization of the gadolinium at the liposomal surface, compared to encapsulated gadolinium, results in an improved MRI signal, which was attributed to a stronger interaction of surface-localized gadolinium with surrounding water molecules (94). However, a disadvantage of surface exposure of the bulky DTPA is that it may sterically hinder the interaction of the liposomes with target cells. Analogously, BBB penetration may be reduced by the polar metal complex at the surface of the carrier. Indeed, thus far no studies have been reported on the use of gadolinium labeled liposomes in brain delivery.

Preparation of iron-labeled liposomes, based on the encapsulation of iron oxide nanoparticles, has also been described (95,96). Recently, also polymersomes have been labeled with magnetic nanoparticles. Depending on the type of initial solvent for the polymer and nanoparticle mixture polymersomes with a shell that is densely packed with nanoparticles can be formed upon subsequent dilution in aqueous medium (97,98). Despite the interesting potential of these magnetic polymerosomes, no data on brain drug delivery using these iron-labeled nanocarriers has been reported so far.

Nanocarrier Labeling with Fluorescent Probes

Liposomes and polymersomes can be readily labeled with lipophilic dyes, such as 6-coumarin, 1,1′-dioctadecyl-3,3,3′,3′-tetramethylindocarbocyanine perchlorate (DiI) and N-(lissamine rhodamine-B sulfonyl)-phosphatidylethanolamine (N-Rh-PE), which become an integral part of the bilayer during liposome/polymersome formation (32,99–101). New fluorescent lipids can be easily made by the esterification of fluorescent dyes with fatty alcohols. For example, the DY-676-C_{18} ester was prepared by esterification of carboxylic acid-modified DY-676 with stearyl alcohol and then applied in the preparation of stable near-infrared fluorescent liposomes (102). Likewise, near-infrared Cy7.5 hydroxysuccinimide was used to label 1,2-dioleoyl-sn-glycero-3-phosphoethanolamine (DOPE) (103). Cy7.5-DOPE containing liposomes were then used to visualize the targeting of liposomes to lung tumors. Many fluorescent dyes are available with several modifications, such as amino, carboxylic acid, maleimide and hydroxysuccinimide groups (for a review see (104)). These functional groups are generally applied for the conjugation of peptides and proteins, including antibodies. However, these functional groups make it also possible to label targeted liposomes, allowing monitoring of improved programmable delivery of the liposomes.

Nanocarrier Labeling with Radioactive Probes

In order to efficiently entrap a radiotracer in the aqueous core of liposomes a trans-chelation method can be used (105). During liposome preparation a strong hydrophilic chelator such as DTPA is encapsulated. Subsequently, liposomes are incubated

with a complex of a weak chelator and a radiotracer such as ^{111}In-oxine. ^{111}In-oxine can pass the lipid bilayer allowing trans-chelation of ^{111}In from the weak oxine complex to the strong DTPA complex. Unbound radiotracer can be removed by dialysis. For the purpose of binding of radiotracer to the surface of liposomes, DTPA-phosphatidylethanolamine (DTPA-PE) is incorporated into the lipid bilayer during liposome preparation (106). Subsequent radiolabeling of the liposome preparation can be performed by trans-chelation as described above. However, it should be noted that chelators are usually highly charged and relatively bulky molecules. When exposed on the surface of liposomes, chelators can therefore readily influence the interaction of the liposomes with the surface of target cells. A recent review on methods for radioactive liposome labeling, describing examples for each labeling strategy, is presented in Phillips *et al.* (107).

There are only few examples of radiolabeling of other nanoparticles that might be potentially used as drug carriers. Solid lipid nanoparticles have been successfully labeled with ^{64}Cu by incorporation of lipid-PEG-BAT, a conjugate between a synthetic pegylated lipid and the copper specific chelator, 6-[p-(bromoacetamido)benzyl]-1,4,8,11-tetraazacyclotetradecane-N,N',N",N"'-tetraacetic acid (BAT), followed by complexation of the radiometal (108). The biodistribution of the solid lipid nanoparticles was quantitatively evaluated both *in vivo* using PET imaging and *ex vivo* by gamma counting. For SPECT imaging, an anti-cancer drug etoposide encapsulated in SLN was labeled with [^{99m}Tc] technetium pertechnetate after reduction with stannous chloride. Polymersomes loaded with Docetaxel were labeled in the same way (109,110). The ^{99m}Tc label was stably incorporated in the nanocarrier both *in vitro* and *in vivo* and allowed successful pharmacokinetics and biodistribution studies. Recently, polymerosomes were functionalized with DTPA and labeled with ^{111}In (111). SPECT imaging could reveal the trafficking of the migration of these polymeroses over time (Fig. 5).

EX VIVO ANALYSIS OF DRUG DELIVERY DEVICE DISTRIBUTION

Ex Vivo Biodistribution

Upon systemic administration of radiolabeled cells or nanocarriers, *ex vivo* biodistribution studies are usually done to determine the fraction of the injected dose that accumulates into the brain. To this end, animals are sacrificed at specific time points after administration of the labeled device, relevant tissues are excised, and radioactivity is determined in the various samples. Recently, a quantitative procedure for determining tissue distribution of nanoparticles, using iron oxide labeled nanoparticles in conjunction with electron spin resonance spectroscopy, has been described (112). In addition, the pharmacokinetics of drug-loaded nanocarriers can be determined by measurement of the drug concentrations in blood samples, taken at multiple time points. In this manner, tissue influx and efflux rate constants can be calculated. This procedure is similar to pharmacokinetic studies of the free drug (113).

Brain accumulation of (non)targeted nanoparticles is typically low compared to the total injected dose, but appears highly variable when different nanoparticles are compared. For example, two hours after i.v. administration of poly (ethyleneglycol)-poly(ε-caprolactone) polymersomes coupled with OX26 antibodies to target vascular endothelial cells into rats, the amount of brain-localized polymersomes was only 0.14% ID/g tissue (101). Similarly, one hour after i.v. administration of nanoparticles composed of a PEG-n-hexadecylcyanoacrylate block-copolymer, the concentration in mouse brain was ~0.2% ID /g tissue, whereas in rat brain the fraction of the injected dose was only 0.005% ID / g tissue. (114). However, in case of nano-PEG-*cross*-PEI nanogels, the fraction within the brain 1 h after i.v. injection in mice reached as high as 2.67% ID/g tissue (115). The high variability of brain accumulation of nanoparticles cannot

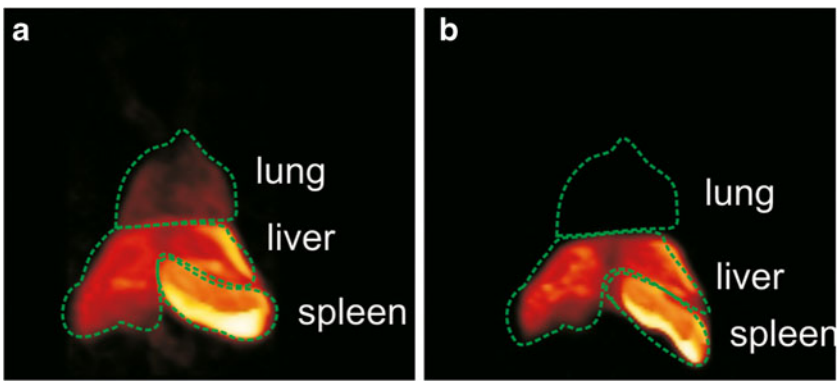

Fig. 5 Volume rendered SPECT of a mouse administered with 220 nm ^{111}In-DTPA labeled polymersomes. (**a**) One hour after intravenous administration of polymersomes with a short blood half life. The radioactivity is visible in the lungs and major blood vessels. Blood vessel radioactivity is due to circulating polymersomes. Radioactivity is also visible in liver and spleen, corresponding to polymersomes trapped by the reticuloendothelial system. (**b**) 24 h after the administration, circulating polymersomes are not visible anymore. Only activity in liver and spleen remains visible.

only be ascribed to intrinsic differences between the nanoparticles and species under investigation, but also to differences between experimental protocols, such as time points of sampling after particle administration, and processing of the brain before particle quantification. For example, when nanoparticle accumulation is quantified for the whole brain, the presence of residual nanoparticles in capillary blood can significantly influence the results. It is therefore critical to perfuse the brain with buffer prior to the isolation to remove residual nanoparticles from the capillaries (32,116–118). Alternatively, total brain nanoparticle content can be corrected for using the (estimated) blood volume and blood nanoparticle concentration (119,120).

In order to discern between the accumulation of drugs in brain parenchyma and vasculature, Triguero *et al.* introduced the capillary depletion method (121). For that purpose, the drug compound is radiolabeled and administered together with a marker compound that is labeled with another radiolabel and known to be retained within the vasculature. At the end of the experiment, the brain is isolated, homogenized, and centrifuged in a density gradient medium. The activity of both radiolabels is measured in the supernatant, serum and pellet fractions that represent parenchyma, blood, and capillaries, respectively. The volume of distribution (V_d) of the test compound in parenchyma and the capillaries can then be calculated. Gutierezz *et al.* used gamma-glutamyl transpeptidase as a vascular marker and showed that in their experimental settings the signal from parenchyma contains approximately 2% signal from vasculature (122). On the other hand, Moos and Morgan used an assay for alkaline phosphatase (EC 3.1.3.1) and showed that vasculature contamination of parenchyma was approximately 16% (7,123). Using the same assay, Gosk *et al.* concluded that the accumulation of OX26-targeted liposomes in the brain parenchymal fraction was clearly a consequence of contamination with liposomes from the capillary fraction. The finding was confirmed by confocal microscopy, which showed that liposomes accumulate in capillaries, but do not cross the BBB (124). Until now brain accumulation of nanoparticles, both targeted and non-targeted, represents only a small fraction of the administered dose. Therefore methods such as capillary depletion and morphological examination are of crucial importance for determining genuine accumulation of nanoparticles into brain parenchyma.

Autoradiography

Autoradiography of radiolabeled drug delivery devices can be used to visualize *ex vivo* the regional distribution of such vehicles in the brain. Sakamoto and Ido (124) used autoradiography to compare the distribution of sulfatide-containing liposomes in brain sections before and after unilateral osmotic opening of the BBB. In case of an intact BBB, the distribution of the liposomes was confined to circumventricular tissues like the pineal body and the regions around the third and lateral ventricles. After osmotic opening of the BBB with a hypertonic mannitol solution, the liposomes showed a homogenous distribution through the whole hemisphere subjected to osmotic opening of the BBB. The distribution of liposomes in the contralateral hemisphere was similar to that observed in case of an intact BBB. However, the resolution obtained by autoradiography is too low to discriminate between localization of liposomes in capillaries and brain parenchyma. Autoradiography was also applied to investigate neural stem cell integration and survival after implantation in the brain. Transduced nerve growth factor secreting neural progenitor cells were labeled with ^{3}H labeled thymidine and injected bilaterally in nucleus basalis and septum. Autoradiography showed that the implanted cells survived, were well integrated in the tissue surrounding the injection site and survived for at least 9 months (125). Although autoradiography is readily applicable and may provide quantitative insight about distribution of drug delivery devices, the technology is currently not widely used in analyzing drug delivery into the brain.

Fluorescence Microscopy

Fluorescence imaging is widely used in brain drug delivery research, because drug delivery devices within the brain, labeled with quantum dots, fluorescent dyes, or expressing fluorescent proteins can be readily detected in tissue slices (11,42,126–128) using high resolution confocal imaging. This approach also allows to distinguish between brain parenchyma and blood vessels, for example by simultaneous visualization of specific markers of endothelial cells, such as CD31, using immunostaining (9,129). An example is shown in Fig. 6).

Analogously, Gosk *et al.* stained brain slices for the basal lamina marker and demonstrated that OX26-targeted liposomes, administered by *in situ* perfusion, were confined to brain endothelial cells, rather than penetrating brain tissue, since no co-localization was seen between the liposomes and laminin (123). Similarly, the relative localization of nanoparticles with respect to glial cells and neurons can be revealed by confocal microscopy, using appropriate markers for these cells (130).

In recent years, an interesting approach has been developed to monitor simultaneously fate of cells and therapeutic efficacy of cell-mediated delivery. The approach relies on the use of dual or triple reporter genes to obtained insight into both cell distribution and expression of therapeutic genes. Following such a procedure, Tang *et al.* stably transfected C17.2 neural stem cells (NSCs) with a plasmid coding for both firefly luciferase (FL) and enhanced green

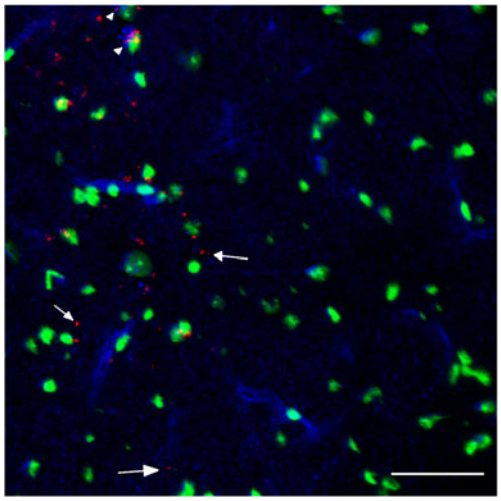

Fig. 6 *In vivo* brain distribution of polymersomes after intracarotid artery injection. BALB/c mice were injected with G23-polymersomes. 24 h later the brains were isolated and immunostained for the endothelial cell marker CD31 (PECAM). G23-polymersomes are found in microvessels, visualized with CD31 (arrowheads), and in brain parenchyma (arrows). Polymersomes are pseudocolored in red, CD31 in blue and nuclei in green. Scale bar, 50 μm. (the image was kindly provided by J. Georgieva and I.S. Zuhorn).

fluorescent protein (eGFP) (11). Bioluminescence was used to monitor the *in vivo* migration of C17.2 NSCs to glioblastomas in brain, while eGFP expression was used for histological confirmation *ex vivo* of the *in vivo* imaging results. The same combination of reporter genes was also used to monitor long-term lentiviral vector-mediated gene expression in the brain (131).

IN VIVO IMAGING OF DRUG DELIVERY DEVICE TRAFFICKING

Several noninvasive imaging techniques have been applied to monitor trafficking of drug delivery devices. Due to the large tissue penetration depth of the imaging signal, PET, SPECT and MRI are applicable both in animals and in humans, making these approaches important tools in translational research. The resolution of optical imaging is relatively poor compared to PET, SPECT and MRI, and results are usually not quantitative due to tissue attenuation and scattering of light. However, *in vivo* bioluminescence and fluorescence imaging have been applied in small animal experiments because of simplicity and low costs (132). Moreover, optical methods are ideally suited to bridge the gap between *in vitro* experiments and animal studies, as *in vivo* imaging results can be easily correlated with *ex vivo* microscopic analysis. Recent developments in optical imaging instrumentation enable interesting new applications in basic research, such as fluorescence tomography and intra-vital microscopy (132). Although there are examples of using *in vivo* imaging techniques to track central nervous system drug delivery devices in humans (48,133), this field is still in its infancy.

Tracking Drug Delivery Devices by MRI

MHP36 stem cells have been labeled with GRID for visualization by MRI. Following their engraftment in the contralateral hemisphere of rat brains with unilateral stroke damage, the spatial distribution and rate of migration of the GRID-labeled cells could be revealed (42,43). MRI demonstrated that 14 days after transplantation the labeled neural stem cells had migrated from the unaffected hemisphere along the corpus callosum to the peri-lesion area.

Similarly, rabbit neonatal NSCs have been labeled with Gd-DTPA in order to non-invasively follow the distribution and migration of cells after acute peripheral nerve traction injury (41). Labeled cells were grafted on distracted sciatic nerves. Serial MRI for up to 70 days after transplantation showed sustained increases in T1 and T2 signals, which was accompanied by improved nerve regeneration. Since transplanted NSCs did not differentiate into neurons or Schwann cells during the time of the experiment, the observed nerve regeneration was attributed to neurotrophic factors released by NSCs.

The migration of Feridex-labeled C17.2 NSCs has been investigated using MRI after intra-ventricular transplantation in a shiverer mouse demyelination model (134). It was possible to follow cell dissemination shortly after transplantation. In most animals the transplanted cells distributed homogenously throughout the ventricular system. An interesting observation was the mismatch between the cellular distribution, as visualized by MRI, and the histological examination, carried out 6 days after stem cell transplantation. Stem cells that were heavily loaded with iron-oxide particles appeared to remain in close proximity of the injection site, while cells that migrated further into the brain parenchyma contained lower amounts of Feridex. The authors concluded that this mismatch may be ascribed to the loss of Feridex by stem cells as a consequence of asymmetric cell division and cell death. MRI-guided focused ultrasound has been used to deliver neural stem cells across the BBB (135). For that purpose, eGFP-expressing embryonic cortical neural progenitor cells were labeled with a SPIO. MRI has subsequently been used to pinpoint relevant brain regions for ultrasound BBB disruption and to non-invasively confirm the entry of stem cells in the brain upon intracarotid administration. The second cell label, eGFP, has been used for confirmation of survival of stem cells *in vivo*, as well as immunohistological confirmation of experimental findings.

Magnetic tumor targeting is a strategy to deliver drugs, carried by magnetic nanoparticles, to a specific location

(136,137). In magnetic targeting, a strong magnet is placed on the body close to the target site, leading to an increase of nanoparticle iron oxide accumulation. The effect of magnetic targeting on the accumulation and clearance of PEGylated and non-PEGylated iron oxide nanoparticles has been examined over time by MRI in a rat 9L-glioma brain tumor model (138,139). The data revealed an increased tumor accumulation of PEGylated compared to non-PEGylated nanoparticles, which could be further promoted (approximately 5-fold) upon magnetic targeting of the iron oxide-loaded nanoparticles. Overall, magnetic targeting was more efficient for the PEGylated nanoparticles.

Convection enhanced delivery (CED) is an experimental method developed in the early 1990s, by which a drug is delivered directly to the brain tumor through a cannula connected to an infusion pump (140). The pump induces positive pressure, thereby dilating the tissue and allowing spreading of the drug. MRI with gadodiamide and fluorescently labeled liposomes has been applied to evaluate real time distribution and retention of liposomes after CED to rats, bearing a 9L-2 tumor (91). Liposomal distribution within brain tissue, as measured by MRI, corresponded well with that observed by *ex vivo* fluorescence imaging. Interestingly, the brain tissue distribution of the gadodiamide liposomes mimicked that of the (commercially available) liposomal drug Doxil and therefore gadodiamide labeled liposomes may serve as a useful marker for the brain tissue distribution of Doxil, administered via CED (91). Real-time MRI monitoring of liposomes loaded with Gadoteridol in combination with CED also provides opportunities for more accurate, site-directed delivery of drug-loaded liposomes to specific brain regions via online control of the administered dose (2,92).

Tracking Drug Delivery Devices by Bioluminescence Imaging

Bioluminescence has been used to compare different delivery methods of neuronal progenitor cells to brain tumors in mice (11). To this end, firefly luciferase transfected C17.2 stem cells were injected into the intra-peritoneal cavity, vasculature, ventricle or brain parenchyma. Bioluminescence imaging demonstrated migration of the cells from parenchyma or ventricle of the healthy hemisphere across the corpus callosum towards the tumor site. However, intravenous administration of the transfected cells resulted in only a modest migration towards the tumor, whereas tumor targeting was virtually absent after intra-peritoneal administration.

Interestingly, when different luciferases with different light emission spectra are used, bioluminescence can also be applied to monitor two processes simultaneously. This approach has been employed for simultaneous monitoring of tumor growth, using glioma cells expressing Renilla luciferase, and migration of neural stem cells, expressing the secreted form of an apoptosis inducing ligand (S-TRAIL) and firefly luciferase (141). After administration to healthy brain, NSCs remain at the site of implantation where they proliferate (11). In contrast, when implanted into the brain of the tumor-bearing mice, S-TRAIL producing NSCs migrate toward the glioma, and significantly reduce tumor growth (141).

Tracking Drug Delivery Devices by Fluorescent Molecular Tomography

Planar fluorescence imaging is generally not used for brain analysis, because the technique does not allow quantification of the signal due to a nonlinear dependence of signal intensity and tissue depth (34,142). However, fluorescence molecular tomography (FMT), a three dimensional quantitative fluorescence imaging technique, has been successfully used in neuroimaging (143). Since FMT does not provide anatomical information, its combined use with a technique such as CT or MRI is preferable. FMT has been applied to track changes of protease activity during brain tumor growth and chemotherapy (144), employing ProSense680 as a fluorescent probe for protease activity. Interestingly, FMT showed changes of tumor protease activity early during chemotherapy, which disappeared at the end of chemotherapy, whereas MRI detected changes in tumor volume only in later stages of chemotherapy. Thus, the combined FMT-MRI imaging approach revealed early chemotherapeutic effects that correctly predicted tumor response.

Beta-amyloid plaques in a murine Alzheimer's disease model have also been analyzed by FMT, using the fluorescent dye oxazine (145). By combining FMT with structural information as obtained by CT, the FMT reconstruction algorithm could be substantially improved, resulting in more precise signal localization.

However, thus far FMT has not been used in studies on drug delivery into the brain. Yet, the principle of the approach, offers a great potential for application in this field.

Tracking Drug Delivery Devices by Intra-Vital Confocal Microscopy

Intra-vital two photon laser scanning microscopy is a highly invasive *in vivo* method that provides the best resolution of all *in vivo* imaging techniques currently available. To study events at the level of microvasculature by intra-vital microscopy, brain cortical microvasculature is exposed. For longitudinal imaging, a cranial window is inserted by removing a piece of skull and replacing it with glass (146). Alternatively, a section of skull can be thinned using a combination of high speed drilling and scraping with a microsurgical blade (147). A disadvantage of the latter method is that thinned bone

grows back again. Recently, Drew *et al.* introduced a procedure to create a stable window in the skull by polished and reinforced thinning of the skull followed by gluing a cover glass to the skull to prevent regrowth (148). In this way, good visibility was achieved for up to 3 months.

Multi-photon laser scanning microscopy in combination with intra-vital microscopy was used to analyze the influence of liposome composition on vascular accumulation in normal tissues and brain tumors (149). Enhancement of the cationic charge of the liposomes resulted in their increased accumulation in tumor vessels, whereas no change in interstitial accumulation was observed. Dreher *et al.* quantified tumor vasculature permeability of macromolecules by monitoring their fluorescence intensity in the vascular and extravascular space (150). They showed that permeability of tumor vasculature was significantly more reduced for dextrans with increasing molecular weight. These studies suggest that confocal intra-vital microscopy has the potential of revealing whether targeted nanoparticles can cross intact BBB or at least that the drug, contained in the transport vehicles, gains access into the brain.

Tracking Drug Delivery Devices by PET or SPECT

PET and SPECT imaging have been used for assessing the outcome of stem cell therapy. For example, [^{18}F]FDOPA PET was used to measure dopamine production in patients with Parkinson's disease, who had received embryonic dopamine cell implantation. One year after surgery, [^{18}F]FDOPA uptake was about 40% higher in patients that underwent transplantation than placebo treated patients. Increased tracer uptake correlated well with clinical symptoms, although primarily in case of patients of 60-years of age or younger (151). Other examples of PET imaging for the indirect assessment of stem cell therapy efficacy have recently been reviewed by Wang *et al.* (152). Only a few examples of direct tracking of stem cells have been published so far. Miletic *et al.* examined *in vivo* killing of 9L glioma cells by bone marrow derived stem cells, expressing the thymidine kinase of herpes simplex virus (HSV-tk) as a suicide gene (127). Apart from bringing about a therapeutic effect, HSV-tk expression in the stem cells can also be used as a reporter gene to localize stem cells *in vivo* by means of PET. To this end an HSV-tk-specific radioactive reporter probe, 9-[4-[^{18}F]fluoro-3-(hydroxymethyl)butyl]guanine ([^{18}F]FHBG), is introduced, 6–7 days after intra-tumoral implantation of the stem cells. The drawback of the method is that [^{18}F]FHBG poorly penetrates the intact BBB, implying that visualization in the brain is only possible when the BBB is damaged, which often accompanies brain tumor development.

The biodistribution of ^{111}In-oxine-labeled human embryonic stem cell-derived neural progenitor cells and rat hippocampal progenitor cells was followed in rats with middle cerebral artery occlusion (153). SPECT showed that cells accumulate in internal organs after administration in the femoral vein. 24 h after carotid artery administration, most cells still accumulated in the peripheral organs, but some human neural progenitor cells were detected in the brain.

Since accumulation of nanoparticles in brain is often low, the signal-to-background ratio is usually poor. Therefore PET and SPECT imaging are hardly used for tracking nanoparticles in the brain. Yet, liposomes carrying hemoglobin have been labeled with 1-[^{18}F]fluoro-3,6-dioxatetracosane for PET imaging in rat brain ischemia induced by thrombosis of the middle cerebral artery (154). The results indicated that liposome encapsulated hemoglobin can reduce the size of infarction, probably as a result of an improvement in the microcirculation and oxygen delivery. Similarly, radiolabeled liposomes were also used to visualize brain tumors by means of PET. The leaky blood vessels in the tumor allowed passive accumulation of liposomes (size of approximately 100 nm) at the tumor site with a relatively low accumulation in the surrounding brain tissue (155). The findings were confirmed by *ex vivo* autoradiography of brain slices.

CONCLUDING REMARKS

Here we have summarized approaches for imaging nanoparticles and stem cells in the brain. For (stem) cell-based delivery devices, imaging can provide information on the location of the labeled cells, cell viability and the extent of therapeutic gene expression over prolonged periods of time. Imaging also allows *in vivo* tracking of nanocarriers over time, provided that the label does not interfere with the distribution of the nanocarrier. Imaging can also provide insight into the stability of nanocarriers and the release of their contents by comparing the distribution of the shell and the contents, when labeled with different markers.

Over the past years, all major imaging modalities, including PET, SPECT, MRI and optical imaging have been applied for monitoring nanocarriers and delivery of associated/entrapped drugs into the brain. Obviously, each modality has its own advantages and limitations, implying that the ideal imaging tool does not exist. The modality of choice strongly depends on the specific experimental and/or therapeutic aims. In addition, there is no ideal all-purpose labeling approach and consequently a labeling strategy should be selected that is most suitable for the specific delivery device involved. In general, however, the labeling agent should ideally be applicable in humans, nontoxic, safe to use, and easy to apply. In addition, the ideal labeling agent has a low background signal *in vivo*, is not released from the drug delivery device, is not affected by environmental factors, including biological fluids, and should not interfere with the crossing of

the delivery vehicle across the BBB. Finally, the lifetime of the label should match the duration of experiment, but the signal of the label should disappear when the delivery device is degraded or stops functioning. Independent of which modality or labeling method is selected, adequate controls are essential, such as controls for the potential release of free tracer from the delivery device, and the localization of the delivery vehicle should be preferably confirmed by histological evidence.

When proper selection and validation of the tracer is performed, imaging of brain drug delivery devices can give an important contribution to research in the brain drug delivery field, including evidence-based optimization of the applied dose and dosing frequency, comparison of administration routes and prediction of therapeutic efficacy, long before the end of treatment. In addition, imaging can provide new insights into causes for failure of particular treatment strategies. Nanocarriers may not reach the brain in adequate quantities, whereas engineered cells may not produce the required therapeutic agent. In these cases it may be advantageous to consider an alternative administration route or drug carrier, rather than pursuing a new lead compound for drug development.

Current progress in *in vivo* molecular imaging includes multimodality imaging approaches. The aim of multimodality imaging is to overcome disadvantages of individual modalities, such as absence of anatomical details or low resolution. An interesting new development in this respect is the introduction of hybrid PET-MRI cameras, both for clinical and preclinical studies. These hybrid cameras not only combine the high sensitivity of PET with the excellent spatial resolution and soft tissue contrast of MRI, but would also allow tracking of dual labeled drug delivery devices. Although the impact of such hybrid imaging devices remains to be determined, it is clear that imaging techniques will remain playing an important role in the development and evaluation of devices that deliver drugs to the brain.

ACKNOWLEDGMENTS AND DISCLOSURES

This work was financially supported by Top Institute Pharma, project T5-105-1: "Nanoscience as a tool for improving bioavailability and blood–brain barrier penetration".

REFERENCES

1. Misra A, Ganesh S, Shahiwala A, Shah SP. Drug delivery to the central nervous system: a review. J Pharm Pharm Sci. 2003;6(2):252–73.
2. Krauze MT, McKnight TR, Yamashita Y, Bringas J, Noble CO, Saito R, *et al.* Real-time visualization and characterization of liposomal delivery into the monkey brain by magnetic resonance imaging. Brain Res Brain Res Protoc. 2005;16(1–3):20–6.
3. Gogel S, Gubernator M, Minger SL. Progress and prospects: stem cells and neurological diseases. Gene Ther. 2011;18(1):1–6.
4. Pardridge WM. Blood–brain barrier drug targeting: the future of brain drug development. Mol Interv. 2003;3(2):90–105. 151.
5. Alvarez-Erviti L, Seow Y, Yin H, Betts C, Lakhal S, Wood MJA. Delivery of siRNA to the mouse brain by systemic injection of targeted exosomes. Nat Biotech. 2011;29(4):341–5.
6. Tiwari SB, Amiji MM. A review of nanocarrier-based CNS delivery systems. Curr Drug Deliv. 2006;3(2):219–32.
7. Moos T, Morgan EH. Restricted transport of anti-transferrin receptor antibody (OX26) through the blood–brain barrier in the rat. J Neurochem. 2001;79(1):119–29.
8. Duffy KR, Pardridge WM. Blood–brain barrier transcytosis of insulin in developing rabbits. Brain Res. 1987;420(1):32–8.
9. Georgieva JV, Brinkhuis RP, Stojanov K, Weijers CAGM, Zuilhof H, Rutjes FPJT, *et al.* Peptide-mediated blood–brain barrier transport of polymersomes. Angew Chem Int Ed Engl. 2012. doi:10.1002/anie.201202001
10. Kanwar JR, Sun X, Punj V, Sriramoju B, Mohan RR, Zhou SF, *et al.* Nanoparticles in the treatment and diagnosis of neurological disorders: untamed dragon with fire power to heal. Nanomedicine. 2012;8(4):399–14.
11. Tang Y, Shah K, Messerli SM, Snyder E, Breakefield X, Weissleder R. *In vivo* tracking of neural progenitor cell migration to glioblastomas. Hum Gene Ther. 2003;14(13):1247–54.
12. Bjugstad KB, Redmond Jr DE, Teng YD, Elsworth JD, Roth RH, Blanchard BC, *et al.* Neural stem cells implanted into MPTP-treated monkeys increase the size of endogenous tyrosine hydroxylase-positive cells found in the striatum: a return to control measures. Cell Transplant. 2005;14(4):183–92.
13. Kelly S, Bliss TM, Shah AK, Sun GH, Ma M, Foo WC, *et al.* Transplanted human fetal neural stem cells survive, migrate, and differentiate in ischemic rat cerebral cortex. Proc Natl Acad Sci U S A. 2004;101(32):11839–44.
14. Muller FJ, Snyder EY, Loring JF. Gene therapy: can neural stem cells deliver? Nat Rev Neurosci. 2006;7(1):75–84.
15. Fischer UM, Harting MT, Jimenez F, Monzon-Posadas WO, Xue H, Savitz SI, *et al.* Pulmonary passage is a major obstacle for intravenous stem cell delivery: the pulmonary first-pass effect. Stem Cells Dev. 2009;18(5):683–92.
16. Harting MT, Jimenez F, Xue H, Fischer UM, Baumgartner J, Dash PK, *et al.* Intravenous mesenchymal stem cell therapy for traumatic brain injury. J Neurosurg. 2009;110(6):1189–97.
17. Stojanov K, de Vries EF, Hoekstra D, van Waarde A, Dierckx RA, Zuhorn IS. [^{18}F]FDG labeling of neural stem cells for *in vivo* cell tracking with positron emission tomography: inhibition of tracer release by phloretin. Mol Imaging. 2012;11(1):1–12
18. Gao J, Dennis JE, Muzic RF, Lundberg M, Caplan AI. The dynamic *in vivo* distribution of bone marrow-derived mesenchymal stem cells after infusion. Cells Tissues Organs. 2001;169(1):12–20.
19. Talbott JF, Cao Q, Bertram J, Nkansah M, Benton RL, Lavik E, *et al.* CNTF promotes the survival and differentiation of adult spinal cord-derived oligodendrocyte precursor cells *in vitro* but fails to promote remyelination *in vivo*. Exp Neurol. 2007;204(1):485–9.
20. Ozeki T, Kaneko D, Hashizawa K, Imai Y, Tagami T, Okada H. Improvement of survival in C6 rat glioma model by a sustained drug release from localized PLGA microspheres in a thermoreversible hydrogel. Int J Pharm. 2012;427(2):299–304.
21. Jones AR, Shusta EV. Blood–brain barrier transport of therapeutics via receptor-mediation. Pharm Res. 2007;24(9):1759–71.
22. Charlton ST, Whetstone J, Fayinka ST, Read KD, Illum L, Davis SS. Evaluation of direct transport pathways of glycine receptor antagonists and an angiotensin antagonist from the nasal cavity to the central nervous system in the rat model. Pharm Res. 2008;25(7):1531–43.
23. Semete B, Booysen L, Lemmer Y, Kalombo L, Katata L, Verschoor J, *et al. In vivo* evaluation of the biodistribution

and safety of PLGA nanoparticles as drug delivery systems. Nanomedicine. 2010;6(5):662–71.
24. Mendez I, Sanchez-Pernaute R, Cooper O, Vinuela A, Ferrari D, Bjorklund L, *et al.* Cell type analysis of functional fetal dopamine cell suspension transplants in the striatum and substantia nigra of patients with Parkinson's disease. Brain. 2005;128(Pt 7):1498–510.
25. Ding H, Inoue S, Ljubimov AV, Patil R, Portilla-Arias J, Hu J, *et al.* Inhibition of brain tumor growth by intravenous poly (beta-L-malic acid) nanobioconjugate with pH-dependent drug release [corrected]. Proc Natl Acad Sci U S A. 2010;107(42):18143–8.
26. Giesel FL, Stroick M, Griebe M, Troster H, von der Lieth CW, Requardt M, *et al.* Gadofluorine m uptake in stem cells as a new magnetic resonance imaging tracking method: an *in vitro* and *in vivo* study. Invest Radiol. 2006;41(12):868–73.
27. Allen TM, Mumbengegwi DR, Charrois GJ. Anti-CD19-targeted liposomal doxorubicin improves the therapeutic efficacy in murine B-cell lymphoma and ameliorates the toxicity of liposomes with varying drug release rates. Clin Cancer Res. 2005;11(9):3567–73.
28. Pirko I, Fricke ST, Johnson AJ, Rodriguez M, Macura SI. Magnetic resonance imaging, microscopy, and spectroscopy of the central nervous system in experimental animals. NeuroRx. 2005;2 (2):250–64.
29. Delikatny EJ, Poptani H. MR techniques for *in vivo* molecular and cellular imaging. Radiol Clin North Am. 2005;43(1):205–20.
30. Choy G, Choyke P, Libutti SK. Current advances in molecular imaging: noninvasive *in vivo* bioluminescent and fluorescent optical imaging in cancer research. Mol Imaging. 2003;2(4):303–12.
31. Weissleder Rand Ntziachristos V. Shedding light onto live molecular targets. Nat Med. 2003;9(1):123–8.
32. Rao J, Dragulescu-Andrasi A, Yao H. Fluorescence imaging *in vivo*: recent advances. Curr Opin Biotechnol. 2007;18(1):17–25.
33. Zacharakis G, Kambara H, Shih H, Ripoll J, Grimm J, Saeki Y, *et al.* Volumetric tomography of fluorescent proteins through small animals *in vivo*. Proc Natl Acad Sci U S A. 2005;102(51):18252–7.
34. Ntziachristos V, Ripoll J, Wang LV, Weissleder R. Looking and listening to light: the evolution of whole-body photonic imaging. Nat Biotechnol. 2005;23(3):313–20.
35. Doyle TC, Burns SM, Contag CH. *In vivo* bioluminescence imaging for integrated studies of infection. Cell Microbiol. 2004;6(4):303–17.
36. Michelini E, Cevenini L, Mezzanotte L, Roda A. Luminescent probes and visualization of bioluminescence. Methods Mol Biol. 2009;574:1–13.
37. Chatziioannou AF. Instrumentation for molecular imaging in preclinical research: micro-PET and Micro-SPECT. Proc Am Thorac Soc. 2005;2(6):533–6. 510–511.
38. Rahmim Aand Zaidi H. PET *versus* SPECT: strengths, limitations and challenges. Nucl Med Commun. 2008;29(3):193–207.
39. Franc BL, Acton PD, Mari C, Hasegawa BH. Small-animal SPECT and SPECT/CT: important tools for preclinical investigation. J Nucl Med. 2008;49(10):1651–63.
40. Shen J, Cheng LN, Zhong XM, Duan XH, Guo RM, Hong GB. Efficient *in vitro* labeling rabbit neural stem cell with paramagnetic Gd-DTPA and fluorescent substance. Eur J Radiol. 2010;75 (3):397–405.
41. Cheng LN, Duan XH, Zhong XM, Guo RM, Zhang F, Zhou CP, *et al.* Transplanted neural stem cells promote nerve regeneration in acute peripheral nerve traction injury: assessment using MRI. AJR Am J Roentgenol. 2011;196(6):1381–7.
42. Modo M, Cash D, Mellodew K, Williams SC, Fraser SE, Meade TJ, *et al.* Tracking transplanted stem cell migration using bifunctional, contrast agent-enhanced, magnetic resonance imaging. Neuroimage. 2002;17(2):803–11.
43. Modo M, Mellodew K, Cash D, Fraser SE, Meade TJ, Price J, *et al.* Mapping transplanted stem cell migration after a stroke: a serial, *in vivo* magnetic resonance imaging study. Neuroimage. 2004;21 (1):311–7.
44. Arbab AS, Yocum GT, Wilson LB, Parwana A, Jordan EK, Kalish H, *et al.* Comparison of transfection agents in forming complexes with ferumoxides, cell labeling efficiency, and cellular viability. Mol Imaging. 2004;3(1):24–32.
45. Modo M, Hoehn M, Bulte JW. Cellular MR imaging. Mol Imaging. 2005;4(3):143–64.
46. Montet-Abou K, Montet X, Weissleder R, Josephson L. Transfection agent induced nanoparticle cell loading. Mol Imaging. 2005;4 (3):165–71.
47. Kustermann E, Himmelreich U, Kandal K, Geelen T, Ketkar A, Wiedermann D, *et al.* Efficient stem cell labeling for MRI studies. Contrast Media Mol Imaging. 2008;3(1):27–37.
48. Zhu J, Zhou L, XingWu F. Tracking neural stem cells in patients with brain trauma. N Engl J Med. 2006;355(22):2376–8.
49. Politi LS, Bacigaluppi M, Brambilla E, Cadioli M, Falini A, Comi G, *et al.* Magnetic-resonance-based tracking and quantification of intravenously injected neural stem cell accumulation in the brains of mice with experimental multiple sclerosis. Stem Cells. 2007;25 (10):2583–92.
50. Walczak P, Kedziorek DA, Gilad AA, Lin S, Bulte JW. Instant MR labeling of stem cells using magnetoelectroporation. Magn Reson Med. 2005;54(4):769–74.
51. Shapiro EM, Skrtic S, Sharer K, Hill JM, Dunbar CE, Koretsky AP. MRI detection of single particles for cellular imaging. Proc Natl Acad Sci U S A. 2004;101(30):10901–6.
52. Hinds KA, Hill JM, Shapiro EM, Laukkanen MO, Silva AC, Combs CA, *et al.* Highly efficient endosomal labeling of progenitor and stem cells with large magnetic particles allows magnetic resonance imaging of single cells. Blood. 2003;102(3):867–72.
53. Michalet X, Pinaud FF, Bentolila LA, Tsay JM, Doose S, Li JJ, *et al.* Quantum dots for live cells, *in vivo* imaging, and diagnostics. Science. 2005;307(5709):538–44.
54. Lin S, Xie X, Patel MR, Yang YH, Li Z, Cao F, *et al.* Quantum dot imaging for embryonic stem cells. BMC Biotechnol. 2007;7:67.
55. So MK, Xu C, Loening AM, Gambhir SS, Rao J. Self-illuminating quantum dot conjugates for *in vivo* imaging. Nat Biotechnol. 2006;24(3):339–43.
56. Pichler A, Prior JL, Piwnica-Worms D. Imaging reversal of multidrug resistance in living mice with bioluminescence: MDR1 P-glycoprotein transports coelenterazine. Proc Natl Acad Sci U S A. 2004;101(6):1702–7.
57. Elhami E, Goertzen AL, Xiang B, Deng J, Stillwell C, Mzengeza S, *et al.* Viability and proliferation potential of adipose-derived stem cells following labeling with a positron-emitting radiotracer. Eur J Nucl Med Mol Imaging. 2011;38(7):1323–34.
58. Botti C, Negri DR, Seregni E, Ramakrishna V, Arienti F, Maffioli L, *et al.* Comparison of three different methods for radiolabelling human activated T lymphocytes. Eur J Nucl Med. 1997;24(5):497–504.
59. Adonai N, Nguyen KN, Walsh J, Iyer M, Toyokuni T, Phelps ME, *et al. Ex vivo* cell labeling with ^{64}Cu-pyruvaldehyde-bis(N4-methylthiosemicarbazone) for imaging cell trafficking in mice with positron-emission tomography. Proc Natl Acad Sci U S A. 2002;99(5):3030–5.
60. Ma B, Hankenson KD, Dennis JE, Caplan AI, Goldstein SA, Kilbourn MR. A simple method for stem cell labeling with fluorine 18. Nucl Med Biol. 2005;32(7):701–5.
61. Li ZB, Chen K, Wu Z, Wang H, Niu G, Chen X. 64Cu-labeled PEGylated polyethylenimine for cell trafficking and tumor imaging. Mol Imaging Biol. 2009;11(6):415–23.
62. Chen K, Miao Z, Cheng Z. *In vivo* PET imaging to track mesenchymal stem cells labelled with copper-64-pyruvaldehyde-bis (N4-methylthiosemicarbazone). J Nucl Med Meeting Abstracts. 2011;52(1_MeetingAbstracts):521.

63. Bhargava KK, Gupta RK, Nichols KJ, Palestro CJ. *In vitro* human leukocyte labeling with ^{64}Cu: an intraindividual comparison with ^{111}In-oxine and ^{18}F-FDG. Nucl Med Biol. 2009;36(5):545–9.
64. Barbash IM, Chouraqui P, Baron J, Feinberg MS, Etzion S, Tessone A, *et al.* Systemic delivery of bone marrow-derived mesenchymal stem cells to the infarcted myocardium: feasibility, cell migration, and body distribution. Circulation. 2003;108(7):863–8.
65. Nowak B, Weber C, Schober A, Zeiffer U, Liehn EA, von Hundelshausen P, *et al.* Indium-111 oxine labelling affects the cellular integrity of haematopoietic progenitor cells. Eur J Nucl Med Mol Imaging. 2007;34(5):715–21.
66. Jin Y, Kong H, Stodilka RZ, Wells RG, Zabel P, Merrifield PA, *et al.* Determining the minimum number of detectable cardiac-transplanted ^{111}In-tropolone-labelled bone-marrow-derived mesenchymal stem cells by SPECT. Phys Med Biol. 2005;50(19):4445–55.
67. Bindslev L, Haack-Sorensen M, Bisgaard K, Kragh L, Mortensen S, Hesse B, *et al.* Labelling of human mesenchymal stem cells with indium-111 for SPECT imaging: effect on cell proliferation and differentiation. Eur J Nucl Med Mol Imaging. 2006;33(10):1171–7.
68. Aicher A, Brenner W, Zuhayra M, Badorff C, Massoudi S, Assmus B, *et al.* Assessment of the tissue distribution of transplanted human endothelial progenitor cells by radioactive labeling. Circulation. 2003;107(16):2134–9.
69. Brenner W, Aicher A, Eckey T, Massoudi S, Zuhayra M, Koehl U, *et al.* ^{111}In-labeled CD34+ hematopoietic progenitor cells in a rat myocardial infarction model. J Nucl Med. 2004;45(3):512–8.
70. Kuyama J, McCormack A, George AJ, Heelan BT, Osman S, Batchelor JR, *et al.* Indium-111 labelled lymphocytes: isotope distribution and cell division. Eur J Nucl Med. 1997;24(5):488–96.
71. Eggert AA, Schreurs MW, Boerman OC, Oyen WJ, de Boer AJ, Punt CJ, *et al.* Biodistribution and vaccine efficiency of murine dendritic cells are dependent on the route of administration. Cancer Res. 1999;59(14):3340–5.
72. Bestor TH. Gene silencing as a threat to the success of gene therapy. J Clin Invest. 2000;105(4):409–11.
73. Gilad AA, Ziv K, McMahon MT, van Zijl PC, Neeman M, Bulte JW. MRI reporter genes. J Nucl Med. 2008;49(12):1905–8.
74. Cohen B, Dafni H, Meir G, Harmelin A, Neeman M. Ferritin as an endogenous MRI reporter for noninvasive imaging of gene expression in C6 glioma tumors. Neoplasia. 2005;7(2):109–17.
75. Genove G, DeMarco U, Xu H, Goins WF, Ahrens ET. A new transgene reporter for *in vivo* magnetic resonance imaging. Nat Med. 2005;11(4):450–4.
76. Nakamura C, Burgess JG, Sode K, Matsunaga T. An iron-regulated gene, magA, encoding an iron transport protein of Magnetospirillum sp. strain AMB-1. J Biol Chem. 1995;270 (47):28392–6.
77. Nakamura C, Kikuchi T, Burgess JG, Matsunaga T. Iron-regulated expression and membrane localization of the magA protein in Magnetospirillum sp. strain AMB-1. J Biochem. 1995;118(1):23–7.
78. Zurkiya O, Chan AW, Hu X. MagA is sufficient for producing magnetic nanoparticles in mammalian cells, making it an MRI reporter. Magn Reson Med. 2008;59(6):1225–31.
79. Boulnois J-L. Photophysical processes in recent medical laser developments: a review. Lasers Med Sci. 1986;1(1):47–66.
80. Deliolanis NC, Wurdinger T, Pike L, Tannous BA, Breakefield XO, Weissleder R, *et al. In vivo* tomographic imaging of red-shifted fluorescent proteins. Biomed Opt Express. 2011;2(4):887–900.
81. Roda A, Guardigli M, Michelini E, Mirasoli M. Nanobioanalytical luminescence: forster-type energy transfer methods. Anal Bioanal Chem. 2009;393(1):109–23.
82. de Almeida PE, van Rappard JR, Wu JC. *In vivo* bioluminescence for tracking cell fate and function. Am J Physiol Heart Circ Physiol. 2011;301(3):H663–71.
83. Sher F, van Dam G, Boddeke E, Copray S. Bioluminescence imaging of Olig2-neural stem cells reveals improved engraftment in a demyelination mouse model. Stem Cells. 2009;27(7):1582–91.
84. Zhang Y, Bressler JP, Neal J, Lal B, Bhang HE, Laterra J, *et al.* ABCG2/BCRP expression modulates D-Luciferin based bioluminescence imaging. Cancer Res. 2007;67(19):9389–97.
85. Meighen EA. Molecular biology of bacterial bioluminescence. Microbiol Rev. 1991;55(1):123–42.
86. Close DM, Patterson SS, Ripp S, Baek SJ, Sanseverino J, Sayler GS. Autonomous bioluminescent expression of the bacterial luciferase gene cassette (lux) in a mammalian cell line. PLoS One. 2010;5(8):e12441.
87. Acton PD, Zhou R. Imaging reporter genes for cell tracking with PET and SPECT. Q J Nucl Med Mol Imaging. 2005;49(4):349–60.
88. Vandeputte C, Evens N, Toelen J, Deroose CM, Bosier B, Ibrahimi A, *et al.* A PET brain reporter gene system based on type 2 cannabinoid receptors. J Nucl Med. 2011;52(7):1102–9.
89. Maresz K, Carrier EJ, Ponomarev ED, Hillard CJ, Dittel BN. Modulation of the cannabinoid CB2 receptor in microglial cells in response to inflammatory stimuli. J Neurochem. 2005;95 (2):437–45.
90. Unger EC, MacDougall P, Cullis P, Tilcock C. Liposomal Gd-DTPA: effect of encapsulation on enhancement of hepatoma model by MRI. Magn Reson Imaging. 1989;7(4):417–23.
91. Saito R, Bringas JR, McKnight TR, Wendland MF, Mamot C, Drummond DC, *et al.* Distribution of liposomes into brain and rat brain tumor models by convection-enhanced delivery monitored with magnetic resonance imaging. Cancer Res. 2004;64(7):2572–9.
92. Saito R, Krauze MT, Bringas JR, Noble C, McKnight TR, Jackson P, *et al.* Gadolinium-loaded liposomes allow for real-time magnetic resonance imaging of convection-enhanced delivery in the primate brain. Exp Neurol. 2005;196(2):381–9.
93. Kabalka G, Buonocore E, Hubner K, Moss T, Norley N, Huang L. Gadolinium-labeled liposomes: targeted MR contrast agents for the liver and spleen. Radiology. 1987;163(1):255–8.
94. Kozlowska D, Foran P, MacMahon P, Shelly MJ, Eustace S, O'Kennedy R. Molecular and magnetic resonance imaging: the value of immunoliposomes. Adv Drug Deliv Rev. 2009;61 (15):1402–11.
95. Elmi MM, Sarbolouki MN. A simple method for preparation of immuno-magnetic liposomes. Int J Pharm. 2001;215(1–2):45–50.
96. Martina MS, Fortin JP, Menager C, Clement O, Barratt G, Grabielle-Madelmont C, *et al.* Generation of superparamagnetic liposomes revealed as highly efficient MRI contrast agents for *in vivo* imaging. J Am Chem Soc. 2005;127(30):10676–85.
97. Hickey RJ, Haynes AS, Kikkawa JM, Park SJ. Controlling the self-assembly structure of magnetic nanoparticles and amphiphilic block-copolymers: from micelles to vesicles. J Am Chem Soc. 2011;133(5):1517–25.
98. Sanson C, Diou O, Thevenot J, Ibarboure E, Soum A, Brulet A, *et al.* Doxorubicin loaded magnetic polymersomes: theranostic nanocarriers for MR imaging and magneto-chemotherapy. ACS Nano. 2011;5(2):1122–40.
99. Hadaczek P, Yamashita Y, Mirek H, Tamas L, Bohn MC, Noble C, *et al.* The "perivascular pump" driven by arterial pulsation is a powerful mechanism for the distribution of therapeutic molecules within the brain. Mol Ther. 2006;14(1):69–78.
100. Lu W, Zhang Y, Tan YZ, Hu KL, Jiang XG, Fu SK. Cationic albumin-conjugated pegylated nanoparticles as novel drug carrier for brain delivery. J Control Release. 2005;107(3):428–48.
101. Pang Z, Lu W, Gao H, Hu K, Chen J, Zhang C, *et al.* Preparation and brain delivery property of biodegradable polymersomes conjugated with OX26. J Control Release. 2008;128(2):120–7.

102. Deissler V, Ruger R, Frank W, Fahr A, Kaiser WA, Hilger I. Fluorescent liposomes as contrast agents for *in vivo* optical imaging of edemas in mice. Small. 2008;4(8):1240–6.
103. He X, Na MH, Kim JS, Lee GY, Park JY, Hoffman AS, *et al.* A novel peptide probe for imaging and targeted delivery of liposomal doxorubicin to lung tumor. Mol Pharm. 2011;8(2):430–8.
104. Nobs L, Buchegger F, Gurny R, Allemann E. Current methods for attaching targeting ligands to liposomes and nanoparticles. J Pharm Sci. 2004;93(8):1980–92.
105. Harrington KJ, Rowlinson-Busza G, Syrigos KN, Uster PS, Vile RG, Stewart JS. Pegylated liposomes have potential as vehicles for intratumoral and subcutaneous drug delivery. Clin Cancer Res. 2000;6(6):2528–37.
106. Levchenko TS, Rammohan R, Lukyanov AN, Whiteman KR, Torchilin VP. Liposome clearance in mice: the effect of a separate and combined presence of surface charge and polymer coating. Int J Pharm. 2002;240(1–2):95–102.
107. Phillips WT, Goins BA, Bao A. Radioactive liposomes. Wiley Interdiscip Rev Nanomed Nanobiotechnol. 2009;1(1):69–83.
108. Andreozzi E, Seo JW, Ferrara K, Louie A. Novel method to label solid lipid nanoparticles with 64cu for positron emission tomography imaging. Bioconjug Chem. 2011;22(4):808–18.
109. Harivardhan Reddy L, Sharma RK, Chuttani K, Mishra AK, Murthy RS. Influence of administration route on tumor uptake and biodistribution of etoposide loaded solid lipid nanoparticles in Dalton's lymphoma tumor bearing mice. J Control Release. 2005;105(3):185–98.
110. Upadhyay KK, Bhatt AN, Castro E, Mishra AK, Chuttani K, Dwarakanath BS, *et al. In vitro* and *in vivo* evaluation of docetaxel loaded biodegradable polymersomes. Macromol Biosci. 2010;10 (5):503–12.
111. Brinkhuis RP, Stojanov K, Laverman P, Eilander J, Zuhorn IS, Rutjes FP, *et al.* Size dependent biodistribution and SPECT imaging of ^{111}In-labeled polymersomes. Bioconjug Chem. 2012. doi:10.1021/bc200578s
112. Chertok B, Cole AJ, David AE, Yang VC. Comparison of electron spin resonance spectroscopy and inductively-coupled plasma optical emission spectroscopy for biodistribution analysis of iron-oxide nanoparticles. Mol Pharm. 2010;7(2):375–85.
113. Wenger Y, Schneider 2nd RJ, Reddy GR, Kopelman R, Jolliet O, Philbert MA. Tissue distribution and pharmacokinetics of stable polyacrylamide nanoparticles following intravenous injection in the rat. Toxicol Appl Pharmacol. 2011;251(3):181–90.
114. Calvo P, Gouritin B, Chacun H, Desmaele D, D'Angelo J, Noel JP, *et al.* Long-circulating PEGylated polycyanoacrylate nanoparticles as new drug carrier for brain delivery. Pharm Res. 2001;18(8):1157–66.
115. Vinogradov SV, Batrakova EV, Kabanov AV. Nanogels for oligonucleotide delivery to the brain. Bioconjug Chem. 2004;15(1):50–60.
116. Costantino L, Gandolfi F, Tosi G, Rivasi F, Vandelli MA, Forni F. Peptide-derivatized biodegradable nanoparticles able to cross the blood–brain barrier. J Control Release. 2005;108(1):84–96.
117. Weiss CK, Kohnle MV, Landfester K, Hauk T, Fischer D, Schmitz-Wienke J, *et al.* The first step into the brain: uptake of NIO-PBCA nanoparticles by endothelial cells *in vitro* and *in vivo*, and direct evidence for their blood–brain barrier permeation. ChemMedChem. 2008;3(9):1395–403.
118. Zensi A, Begley D, Pontikis C, Legros C, Mihoreanu L, Wagner S, *et al.* Albumin nanoparticles targeted with Apo E enter the CNS by transcytosis and are delivered to neurones. J Control Release. 2009;137(1):78–86.
119. Khor SP, Mayersohn M. Potential error in the measurement of tissue to blood distribution coefficients in physiological pharmacokinetic modeling. Residual tissue blood. I. Theoretical considerations. Drug Metab Dispos. 1991;19(2):478–85.
120. Khor SP, Bozigian H, Mayersohn M. Potential error in the measurement of tissue to blood distribution coefficients in physiological pharmacokinetic modeling. Residual tissue blood. II. Distribution of phencyclidine in the rat. Drug Metab Dispos. 1991;19(2):486–90.
121. Triguero D, Buciak J, Pardridge WM. Capillary depletion method for quantification of blood–brain barrier transport of circulating peptides and plasma proteins. J Neurochem. 1990;54(6):1882–8.
122. Gutierrez EG, Banks WA, Kastin AJ. Murine tumor necrosis factor alpha is transported from blood to brain in the mouse. J Neuroimmunol. 1993;47(2):169–76.
123. Gosk S, Vermehren C, Storm G, Moos T. Targeting anti-transferrin receptor antibody (OX26) and OX26-conjugated liposomes to brain capillary endothelial cells using *in situ* perfusion. J Cereb Blood Flow Metab. 2004;24(11):1193–204.
124. Sakamoto Aand Ido T. Liposome targeting to rat brain: effect of osmotic opening of the blood–brain barrier. Brain Res. 1993;629 (1):171–5.
125. Martinez-Serrano Aand Bjorklund A. *Ex vivo* nerve growth factor gene transfer to the basal forebrain in presymptomatic middle-aged rats prevents the development of cholinergic neuron atrophy and cognitive impairment during aging. Proc Natl Acad Sci U S A. 1998;95(4):1858–63.
126. Sugiyama T, Kuroda S, Osanai T, Shichinohe H, Kuge Y, Ito M, *et al.* Near-infrared fluorescence labeling allows noninvasive tracking of bone marrow stromal cells transplanted into rat infarct brain. Neurosurgery. 2011;68(4):1036–47. discussion 1047.
127. Miletic H, Fischer Y, Litwak S, Giroglou T, Waerzeggers Y, Winkeler A, *et al.* Bystander killing of malignant glioma by bone marrow-derived tumor-infiltrating progenitor cells expressing a suicide gene. Mol Ther. 2007;15(7):1373–81.
128. Zhao D, Najbauer J, Garcia E, Metz MZ, Gutova M, Glackin CA, *et al.* Neural stem cell tropism to glioma: critical role of tumor hypoxia. Mol Cancer Res. 2008;6(12):1819–29.
129. Rao KS, Reddy MK, Horning JL, Labhasetwar V. TAT-conjugated nanoparticles for the CNS delivery of anti-HIV drugs. Biomaterials. 2008;29(33):4429–38.
130. Sousa F, Mandal S, Garrovo C, Astolfo A, Bonifacio A, Latawiec D, *et al.* Functionalized gold nanoparticles: a detailed *in vivo* multimodal microscopic brain distribution study. Nanoscale. 2010;2(12):2826–34.
131. Deroose CM, Reumers V, Gijsbers R, Bormans G, Debyser Z, Mortelmans L, *et al.* Noninvasive monitoring of long-term lentiviral vector-mediated gene expression in rodent brain with bioluminescence imaging. Mol Ther. 2006;14(3):423–31.
132. Massoud TF, Gambhir SS. Molecular imaging in living subjects: seeing fundamental biological processes in a new light. Genes Dev. 2003;17(5):545–80.
133. Fand Callera, de Melo CM. Magnetic resonance tracking of magnetically labeled autologous bone marrow CD34+ cells transplanted into the spinal cord via lumbar puncture technique in patients with chronic spinal cord injury: CD34+ cells' migration into the injured site. Stem Cells Dev. 2007;16(3):461–6.
134. Walczak P, Kedziorek DA, Gilad AA, Barnett BP, Bulte JW. Applicability and limitations of MR tracking of neural stem cells with asymmetric cell division and rapid turnover: the case of the shiverer dysmyelinated mouse brain. Magn Reson Med. 2007;58 (2):261–9.
135. Burgess A, Ayala-Grosso CA, Ganguly M, Jordao JF, Aubert I, Hynynen K. Targeted delivery of neural stem cells to the brain using MRI-guided focused ultrasound to disrupt the blood–brain barrier. PLoS One. 2011;6(11):e27877.
136. Alexiou C, Arnold W, Klein RJ, Parak FG, Hulin P, Bergemann C, *et al.* Locoregional cancer treatment with magnetic drug targeting. Cancer Res. 2000;60(23):6641–8.
137. Lubbe AS, Alexiou C, Bergemann C. Clinical applications of magnetic drug targeting. J Surg Res. 2001;95(2):200–6.

138. Cole AJ, David AE, Wang J, Galban CJ, Hill HL, Yang VC. Polyethylene glycol modified, cross-linked starch-coated iron oxide nanoparticles for enhanced magnetic tumor targeting. Biomaterials. 2011;32(8):2183–93.
139. Cole AJ, David AE, Wang J, Galban CJ, Yang VC. Magnetic brain tumor targeting and biodistribution of long-circulating PEG-modified, cross-linked starch-coated iron oxide nanoparticles. Biomaterials. 2011;32(26):6291–301.
140. Raghavan R, Brady ML, Rodriguez-Ponce MI, Hartlep A, Pedain C, Sampson JH. Convection-enhanced delivery of therapeutics for brain disease, and its optimization. Neurosurg Focus. 2006;20(4):E12.
141. Shah K, Bureau E, Kim DE, Yang K, Tang Y, Weissleder R, *et al.* Glioma therapy and real-time imaging of neural precursor cell migration and tumor regression. Ann Neurol. 2005;57(1):34–41.
142. Billinton Nand Knight AW. Seeing the wood through the trees: a review of techniques for distinguishing green fluorescent protein from endogenous autofluorescence. Anal Biochem. 2001;291(2):175–97.
143. Ntziachristos V. Fluorescence molecular imaging. Annu Rev Biomed Eng. 2006;8:1–33.
144. McCann CM, Waterman P, Figueiredo JL, Aikawa E, Weissleder R, Chen JW. Combined magnetic resonance and fluorescence imaging of the living mouse brain reveals glioma response to chemotherapy. Neuroimage. 2009;45(2):360–9.
145. Hyde D, de Kleine R, MacLaurin SA, Miller E, Brooks DH, Krucker T, *et al.* Hybrid FMT-CT imaging of amyloid-beta plaques in a murine Alzheimer's disease model. Neuroimage. 2009;44(4):1304–11.
146. Levasseur JE, Wei EP, Raper AJ, Kontos AA, Patterson JL. Detailed description of a cranial window technique for acute and chronic experiments. Stroke. 1975;6(3):308–17.
147. Grutzendler J, Kasthuri N, Gan WB. Long-term dendritic spine stability in the adult cortex. Nature. 2002;420(6917):812–6.
148. Drew PJ, Shih AY, Driscoll JD, Knutsen PM, Blinder P, Davalos D, *et al.* Chronic optical access through a polished and reinforced thinned skull. Nat Methods. 2010;7(12):981–4.
149. Campbell RB, Fukumura D, Brown EB, Mazzola LM, Izumi Y, Jain RK, *et al.* Cationic charge determines the distribution of liposomes between the vascular and extravascular compartments of tumors. Cancer Res. 2002;62(23):6831–6.
150. Dreher MR, Liu W, Michelich CR, Dewhirst MW, Yuan F, Chilkoti A. Tumor vascular permeability, accumulation, and penetration of macromolecular drug carriers. J Natl Cancer Inst. 2006;98(5):335–44.
151. Nakamura T, Dhawan V, Chaly T, Fukuda M, Ma Y, Breeze R, *et al.* Blinded positron emission tomography study of dopamine cell implantation for Parkinson's disease. Ann Neurol. 2001;50(2):181–7.
152. Wang J, Tian M, Zhang H. PET molecular imaging in stem cell therapy for neurological diseases. Eur J Nucl Med Mol Imaging. 2011;38(10):1926–38.
153. Lappalainen RS, Narkilahti S, Huhtala T, Liimatainen T, Suuronen T, Narvanen A, *et al.* The SPECT imaging shows the accumulation of neural progenitor cells into internal organs after systemic administration in middle cerebral artery occlusion rats. Neurosci Lett. 2008;440(3):246–50.
154. Urakami T, Kawaguchi AT, Akai S, Hatanaka K, Koide H, Shimizu K, *et al. In vivo* distribution of liposome-encapsulated hemoglobin determined by positron emission tomography. Artif Organs. 2009;33(2):164–8.
155. Oku N, Yamashita M, Katayama Y, Urakami T, Hatanaka K, Shimizu K, *et al.* PET imaging of brain cancer with positron emitter-labeled liposomes. Int J Pharm. 2011;403(1–2):170–7.
156. Liu HS, Jan MS, Chou CK, Chen PH, Ke NJ. Is green fluorescent protein toxic to the living cells? Biochem Biophys Res Commun. 1999;260(3):712–7.
157. Klein RL, Dayton RD, Leidenheimer NJ, Jansen K, Golde TE, Zweig RM. Efficient neuronal gene transfer with AAV8 leads to neurotoxic levels of tau or green fluorescent proteins. Mol Ther. 2006;13(3):517–27.
158. Davidson MW, Campbell RE. Engineered fluorescent proteins: innovations and applications. Nat Methods. 2009;6(10):713–7.
159. Tiffen JC, Bailey CG, Ng C, Rasko JE, Holst J. Luciferase expression and bioluminescence does not affect tumor cell growth *in vitro or in vivo. Mol Cancer. 2010;9:299.*
160. Fernandez P, Bordenave L, Celerier C, Bareille R, Brouillaud B, Basse-Cathalinat B. A novel potential application for ^{99m}Tc-HMPAO: endothelial cell labeling for *in vitro* investigation of cell-biomaterial interactions. J Nucl Med. 1999;40(10):1756–63.
161. Deliolanis NC, Kasmieh R, Wurdinger T, Tannous BA, Shah K, Ntziachristos V. Performance of the red-shifted fluorescent proteins in deep-tissue molecular imaging applications. J Biomed Opt. 2008;13(4):044008.
162. Patterson GH, Knobel SM, Sharif WD, Kain SR, Piston DW. Use of the green fluorescent protein and its mutants in quantitative fluorescence microscopy. Biophys J. 1997;73(5):2782–90.
163. Shaner NC, Campbell RE, Steinbach PA, Giepmans BN, Palmer AE, Tsien RY. Improved monomeric red, orange and yellow fluorescent proteins derived from Discosoma sp. red fluorescent protein. Nat Biotechnol. 2004;22(12):1567–72.
164. Wang L, Jackson WC, Steinbach PA, Tsien RY. Evolution of new nonantibody proteins via iterative somatic hypermutation. Proc Natl Acad Sci U S A. 2004;101(48):16745–9.
165. Shcherbo D, Merzlyak EM, Chepurnykh TV, Fradkov AF, Ermakova GV, Solovieva EA, *et al.* Bright far-red fluorescent protein for whole-body imaging. Nat Methods. 2007;4(9):741–6.
166. Fraga H. Firefly luminescence: a historical perspective and recent developments. Photochem Photobiol Sci. 2008;7(2):146–58.
167. Wood KV, Lam YA, Seliger HH, McElroy WD. Complementary DNA coding click beetle luciferases can elicit bioluminescence of different colors. Science. 1989;244(4905):700–2.
168. Lorenz WW, McCann RO, Longiaru M, Cormier MJ. Isolation and expression of a cDNA encoding Renilla reniformis luciferase. Proc Natl Acad Sci U S A. 1991;88(10):4438–42.
169. Loening AM, Wu AM, Gambhir SS. Red-shifted Renilla reniformis luciferase variants for imaging in living subjects. Nat Methods. 2007;4(8):641–3.
170. Ji X, Cheng L, Wei F, Li H, Wang M, Tian Y, *et al.* Noninvasive visualization of retinoblastoma growth and metastasis via bioluminescence imaging. Invest Ophthalmol Vis Sci. 2009;50(12):5544–51.
171. Tannous BA, Kim DE, Fernandez JL, Weissleder R, Breakefield XO. Codon-optimized Gaussia luciferase cDNA for mammalian gene expression in culture and *in vivo*. Mol Ther. 2005;11(3):435–43.
172. Tjuvajev JG, Doubrovin M, Akhurst T, Cai S, Balatoni J, Alauddin MM, *et al.* Comparison of radiolabeled nucleoside probes (FIAU, FHBG, and FHPG) for PET imaging of HSV1-tk gene expression. J Nucl Med. 2002;43(8):1072–83.
173. MacLaren DC, Gambhir SS, Satyamurthy N, Barrio JR, Sharfstein S, Toyokuni T, *et al.* Repetitive, non-invasive imaging of the dopamine D2 receptor as a reporter gene in living animals. Gene Ther. 1999;6(5):785–91.
174. Auricchio A, Acton PD, Hildinger M, Louboutin JP, Plossl K, O'Connor E, *et al. In vivo* quantitative noninvasive imaging of gene transfer by single-photon emission computerized tomography. Hum Gene Ther. 2003;14(3):255–61.
175. Shin JH, Chung JK, Kang JH, Lee YJ, Kim KI, So Y, *et al.* Noninvasive imaging for monitoring of viable cancer cells using a dual-imaging reporter gene. J Nucl Med. 2004;45(12):2109–15.

176. Zinn KR, Buchsbaum DJ, Chaudhuri TR, Mountz JM, Grizzle WE, Rogers BE. Noninvasive monitoring of gene transfer using a reporter receptor imaged with a high-affinity peptide radiolabeled with 99mTc or 188Re. J Nucl Med. 2000;41(5):887–95.
177. Rogers BE, Chaudhuri TR, Reynolds PN, Della Manna D, Zinn KR. Non-invasive gamma camera imaging of gene transfer using an adenoviral vector encoding an epitope-tagged receptor as a reporter. Gene Ther. 2003;10(2):105–14.
178. Doubrovin M, Ponomarev V, Serganova I, Soghomonian S, Myagawa T, Beresten T, *et al.* Development of a new reporter gene system–dsRed/xanthine phosphoribosyltransferase-xanthine for molecular imaging of processes behind the intact blood–brain barrier. Mol Imaging. 2003;2(2):93–112.